Influence of Energy Exchange Between Air and Liquid Streams on Spray Characteristics and Atomization Efficiency of Water-Air Impinging Jets

Y. Xia*, L. Khezzar, Y. Hardalupas**, M. Alshehhi

Mechanical Engineering Department, Khalifa University of Science and Technology, P. O. Box 2533, Abu Dhabi, United Arab Emirates
(*) School of Engineering, The University of British Columbia, 1137 Alumni Ave, Kelowna, BC V1V 1V7, Canada
(**) Mechanical Engineering Department, Imperial College London, London, UK
Corresponding email address: lyes.khezzar@ku.ac.ae

Abstract

The paper evaluates the interaction between atomization quality and atomization efficiency, which has not been understood, although it is commonly observed that the atomization quality of different atomizers does not improve linearly with addition of energy. The results quantify the energy exchange between the air and liquid streams of a twin water impinging jets atomizer and its consequences on atomization characteristics and explain the behavior of quality and efficiency. The liquid jet breakup length, liquid jets separation distance at the breakup region and spray angles were measured with high speed photography and the droplet characteristics, such as spatial distributions of mean droplet velocities and diameters and normalized liquid volume flux with Phase Doppler Particle Analyzer (PDPA).

The results show that the breakup length decreased and the separation distance of the interacting liquid jets at the geometrical 'impingement' region increased rapidly as Air-to-Liquid Momentum Ratio (ALMR) increased and then remained constant for ALMR>9. Spray angles were different on different planes through the spray and generally decreased with increasing ALMR and were insensitive to the liquid jets impingement angle. The spatial distributions of average droplet size, velocity and normalized liquid volume flux in the sprays became elongated normal to the plane of the two liquid jets for larger liquid flow rates, in agreement with the spray angle in the near nozzle region. The spatially-averaged Sauter Mean Diameter (SMD) of the sprays quantified uniquely the atomization quality and showed, for the first time, that it did not depend on liquid jets impingement angle. The average SMD remained constant beyond ALMR=9, in agreement with the near nozzle characteristics, which was explained by the energy exchange between the two streams, which reached a maximum for ALMR=3 before reducing and remaining constant for ALMR>9.

The atomization efficiency was quantified from the measured spatially-averaged SMD, for the first time, according to formalisms of Lefebvre (1992) and Pizziol et al. (2018). The atomization efficiency of Pizziol et al (2018) increased with the reduction of the liquid flowrate and increase of air flowrate up to Air-to-Liquid mass flowrate Ratio (ALR) of around 0.2 beyond which further increase leads to reduction of efficiency. Although this trend did not agree with Lefebvre, the values of the atomization efficiency of Lefebvre's formalism were around 0.7% of the supplied air kinetic energy, in agreement with the measured energy exchange between the air and liquid streams up to liquid breakup, while the values of Pizziol et al. (2018) were larger, probably due to the additional energy exchange between liquid and gas during secondary ligament breakup.

Key words: Atomization quality; atomization efficiency; air-to-liquid energy exchange; Impinging jets; liquid breakup visualization; droplet sizing; spatially averaged Sauter Mean Diameter

Nomenclature

ALMR	air to liquid momentum ratio ($ALMR = \dot{m}_G U_{imp} / \dot{m}_L U_L$)
ALMFR	air to liquid momentum flux ratio ($ALMFR = \rho_G U_{imp}^2 / 2\rho_L U_L^2$)
C*	factor in Eq. (1)
D_{10}	Arithmetic Mean Diameter
D_a	diameter of the water jet exit nozzle, m
D_L	diameter of the water jet exit nozzle, m
G(x,y)	local volume flux at the location (x,y) of the spray, ml/cm^2/s
ALR	air to liquid mass flowrate ratio (ALR= $\dot{m}_G / \dot{m}_L$)
h	separation distance between the two intact liquid jets at the geometrical impingement point, mm
L	water jet breakup length, mm
$\dot{m}_L$	mass flow rate of liquid, supplied through the two liquid jets, g/min
$\dot{m}_G$	mass flow rate of gas, g/min
Q_L	water volume flow rate, supplied through the two liquid jets, ml/min
Re_L	Reynolds number of liquid jet ($Re_L = \rho_L D_L U_L / \mu_L$)
SKEI	specific kinetic energy increase of the liquid flow, m^2/s^2
RMS	root mean square of the fluctuations of a measured quantity
SMD	Sauter Mean Diameter, μm
$U_{detaching}$	velocity of liquid fragments during detachment at the breakup location, m/s
U_l	Area-averaged liquid velocity at jet exit, m/s
U_G	Area-averaged gas velocity at jet exit, m/s
U_{imp}	magnitude of gas jet flow velocity at the impingement point, m/s
W	axial velocity of a droplet inside the spray, m/s
We	Weber number ($We = \rho_G (U_G - U_L)^2 D_L / \sigma$)
Z	distance from the geometrical impingement point of the two liquid jets to a downstream position, mm
Greek symbols	
ρ_L	liquid density, kg/m^3
ρ_G	gas density, kg/m^3
2θ	angle between the axes of the two water jets, °
α	front view spray angle in plane Y-Z, °
β	side view spray angle in plane X-Z, °
μ	dynamic viscosity, N·s/m^2
σ_L	surface tension between the interface of liquid and gas, N/m
ν_L	kinematic viscosity of liquid, m^2/s

1. Introduction

Due to their relatively high atomization efficiency, twin-impinging liquid jet atomizers have been widely utilized in propulsion systems (Dombrowski and Hooper 1964, Lefebvre 1988; Ramasubramanian et al. 2015). The constant need to improve combustion performance is mainly driven by regulatory measures and efforts towards containing carbon emissions on a global scale, while reducing NO_X and particulate emissions. This calls for improved liquid fuel atomization and ability to control liquid droplet sizes over a wide range of operating conditions. For example, it is a fact that, at part load, the atomization quality of twin impinging liquid jet atomizers can drop and one proposed method to remedy this is to use an additional gas jet (Inoue et al. 2013, Pizziol et al. 2018, Xia et al. 2017, 2018). This paper links the origin of the behavior of the atomization characteristics and the resulting atomization efficiency to the measured energy exchange between the air and liquid streams in the near nozzle region for the first time.

A number of experimental and computational studies on impinging liquid and air jet atomizers were conducted in the past (Boden et al. 1999; Ashgriz 2011; Avulapati and Venkata 2013; Inoue et al. 2013; Prabhakaran and Basavanahalli 2013; Panao and Delgado 2014, Xia et al. 2017; Xia et al. 2018a; Xia et al. 2018b; Pizziol et al. 2018). Avulapati and Ravikrishna (2013) used Particle/Droplet Imaging Analysis (PDIA) to characterize the sprays. Inoue et al. (2013) also carried out a study on this configuration using a high speed camera for visualization and a combination of CCD camera and pulsed YAG laser for droplet size measurement, together with numerical analysis. Results indicated that the atomization is significantly enhanced with addition of air mass flowrate equal to 1% of the liquid jets mass flowrate. The ratio of gas to liquid jet dynamic pressure at the impingement region was shown to be the dominant non-dimensional parameter and optimized atomization was obtained when its value was approximately greater than 2. Panao and Delgado (2104) investigated 2 and 3 impinging liquid jet configurations and proposed correlations for D_{10} and SMD and for droplet velocities normalized by the jet exit velocity. Avulapati and Ravikrishna (2105) evaluated the performance of such configuration for the atomization of pure plant oils and showed that air-assist atomizers deliver same level of atomization as conventional Diesel fuel type pressure injectors. Pizziol et al. (2018) studied twin and multiple impinging jets air assisted atomization using laser diffraction to measure the line of sight averaged SMD along a section of the sprays. They proposed a correlation for SMD and showed that the liquid jet diameter had limited effect on SMD confirming findings by Lefebvre (1992) about atomizing air stream impacting a liquid

stream at relatively large angles. They also confirmed that the addition of an air jet leads to breakup dominated by aerodynamic forces as documented by Xia et al. (2017). Xia et al. (2017) performed detailed flow visualization of twin liquid impinging jets and provided local measurements of droplet size and velocity using Phase Doppler Particle Analyzer (PDPA). Local Sauter Mean Diameter (SMD), normalized by the air jet diameter, was found to initially decrease with increase of air-to-liquid mass ratio and air-to-liquid momentum ratio and remained almost constant beyond a certain value. The latter means that the atomization quality does not improve for values of the air-to-liquid mass ratio beyond a certain level and, therefore, the added energy of the atomizing air does not contribute to finer atomization, thus reducing the atomization efficiency of the atomizer. It seems, therefore, logical to link the atomization quality to the atomization efficiency of each atomizer design. However, the energy exchange between the air and liquid streams, which determine these processes, have not been quantified in previous studies.

Several ways have been proposed to characterize the atomization efficiency in airblast atomizers. Generally, these definitions are based on the ratio of the energy required for the atomization, which represents the increase of the liquid surface area over the energy input through the air and liquid streams. For example, in a similar configuration, Avulapati and Ravikrishna (2013) used a definition for effervescent atomization similarity and found a low atomization efficiency of around 0.25%. Lefebvre (1992), after a review of experimental results for twin-liquid atomizers, developed a semi-empirical approach to quantify the atomization efficiency for the resulting sprays from the breakup of planar liquid sheets and round jets being impinged upon by a high velocity air stream. For a round jet, he was able to derive an equation (Eq. (1)) for droplet SMD as a function of the liquid jets nozzle diameter, liquid surface tension and density, kinetic energy of the air stream and the air-to-liquid mass flowrate ratio ALR, defined in Eq. (5).

$$SMD = \frac{3}{\frac{2}{D_L} + \frac{C * \rho_L U_G^2}{4\sigma_L \left(1 + \frac{1}{ALR}\right)}} \tag{1}$$

It is also worth mentioning that Knoll and Sojka (1992) also developed a similar equation to that of Lefebvre for flat liquid sheet with a dependence on the term $(1 + \frac{1}{ALR})$ but using the relative velocity between the liquid and gas streams rather than the gas velocity.

In Eq. (1), C* represents the fraction of the kinetic energy of the air stream being used to increase the liquid surface area during atomization and quantifies the atomization efficiency. In developing the above equation, Lefebvre considered the case of a jet being impinged upon by a gas stream at an appreciable angle noting that, in such situation, the liquid jet is torn into small fragments by the vigorous interaction between the liquid and air streams. As a consequence, it is expected that the ratio of the energy required for atomization to the atomizing air kinetic energy is important for the atomization quality and efficiency but the physics of the energy exchanges were not studied. Using experimental data, obtained by Beck et al. (1991), of mean droplet diameters that were only available for atomized planar liquid sheets and were not spatially averaged over the complete cross-section of the non-axisymmetric sprays at an axial distance from the nozzle exit, Lefebvre (1992) quantified the atomization efficiency (i.e. the constant C* of Eq. (1)) to be around 0.7%. At around the same time and as mentioned above, Knoll and Sojka (1992) in their relation for SMD introduce an equivalent parameter to C* which they termed ε to quantify the fraction of atomizing air that uses all of its energy to increase the surface energy of the droplets. Going beyond a single value for flat liquid sheets, these authors propose a correlation for ε as a function of liquid viscosity, ALR and relative velocity. However, for a round liquid jet, the atomization efficiency was not determined due to lack of droplet sizing measurements in the sprays. This paper remedies this and obtains values of C* for round jets and proposes a correlation, similar to the one proposed by Knoll and Sojka (1992).

Recently, Pizziol et al. (2018) introduced another formalism for the atomization efficiency that relates the final volumetric surface energy of the droplets to the sum of the kinetic energy components of the air jet and the liquid jets. This led to the correlation of Eq. (2):

$$\eta_{atom} = \frac{\left(\frac{6\sigma_L}{SMD}\right)}{\frac{8}{\rho_a}\left(\frac{\dot{m}_G}{\pi D_a^2}\right)^2 + 2\left[\frac{8}{\rho_L}\left(\frac{\dot{m}_L}{\pi D_L^2}\right)^2 + \frac{4\sigma_L}{D_L}\right]} \qquad (2)$$

Pizziol et al. (2018) considered two different types of liquids and several liquid and air mass flow rates and found that the maximum values of atomization efficiency varied between 6 and 8.5%. However, the mean droplet size used in their calculations was a spatially-averaged value along a line of sight of the laser beam of a laser diffraction instrument through the central region

of non-axisymmetric sprays. Hence, the droplets that were not crossing the laser beam, but contributed to the change of the surface area of the liquid, were not taken into account. Therefore, the quantitative evaluation of the atomization efficiency of an atomizer design is still open and the current research attempts to improve this deficiency, while it quantifies the energy exchange between the air and liquid streams.

Assessment of the atomization quality using local values of the SMD, as used by most of the previous studies, may not be adequate, since it does not represent all the droplets present in the spray. This can be worse for non-axisymmetric sprays, generated by the impingement of an air stream on liquid streams at an angle (e.g. Lefebvre 1992, Xia et al. 2017, Avulapati and Ravikrishna 2013, Pizziol et al. 2018)). Avulapati and Ravikrishna (2013) used local mean diameters and Pizziol et al. (2018) used line of sight average droplet size measurements limited to only a small fraction of the sprays.

The current paper addresses several objectives. Firstly, the work of Xia et al. (2017) is extended by measuring the complete spatial distribution of the spray characteristics. This allows the quantification of the liquid flux-weighted spatially-averaged SMD (which is defined in Eq. (8)) over a cross-section of the sprays in order to evaluate the atomization quality and efficiency as a function of the liquid jets impinging angle and Air-to-Liquid Momentum Ratio (ALMR) by using all the droplets in a spray for the first time.

Since the liquid breakup is dominated by aerodynamic interactions between the liquid and air streams, as documented qualitatively by Inoue et al. (2013), Pizziol et al. (2018) and Xia et al. (2017, 2018), the characteristics of the downstream sprays depend on the near nozzle breakup process. The quantification of the breakup characteristics is required to understand the exchange of energy between the air and the liquid streams and its consequence on the atomization quality and efficiency. Therefore, the second objective is the extension of the work of Xia et al. (2017) to quantify the breakup length of the 'impinging' liquid jets (L) and their separation distance (h) at the 'geometrical' impingement point, see Fig. 3. The third objective of the paper is the quantification, for the first time, of the energy exchange between the air and liquid streams upstream of the breakup point, which explains the behavior of the atomization quality of the downstream droplet sizes and the atomization efficiency, as defined by Eq. (1) of Lefebvre (1992) and Eq. (2) of Pizziol et al. (2018).

The remaining manuscript provides a description of the experimental setup, measurement techniques and associated uncertainties, followed by the presentation of the results and conclusions.

2. Experimental setup

Spray visualization and simultaneous measurements of droplet size, velocity and liquid volume flux were carried out using high speed photography and PDPA respectively at an ambient room temperature of 20 ºC and atmospheric pressure.

Figure 1 presents the schematic of the experimental setup. The spray is generated by the impingement of two water jets supplied by two magnetically coupled centrifugal pumps and an impinging air jet, supplied by a centralized compressor system, which gives a stable air supply. The atomizer, shown in Fig. 2, consists of three stainless steel tubes of 0.686 mm internal diameter for the water jets and 1 mm for the air jet. The lengths of water and air tubes are 152.4 and 304.8 mm to guarantee fully developed flow conditions at the nozzle exits. The distance between the nozzle exits and the geometrical impingement point *O* is 10 mm for the water and 12 mm for air flows. The angle between the two water jets can be varied, while keeping the air jet vertical.

A high speed camera recorded the liquid flow during breakup with the help of an LED matrix providing back-lit illumination. The recording speed was set up at 15,000 kHz, which provided appropriate temporal resolution to record the process. The images were processed with ImageJ software. The image processing allows the quantification of the instantaneous liquid breakup length, *L*, and separation distance between the two liquid jets, *h*, and Fig. 3 provides example images that indicate the definition of these quantities.

The mean value and the standard deviation of the fluctuations of the breakup length were quantified from 50 instantaneous images of the primary atomization, captured for each operating condition, which led to uncertainties of 2% for the mean and 6% for the standard deviation of the fluctuations. The separation distance between the liquid jets, *h*, is also quantified from 50 instantaneous images for each flow condition, which lead to uncertainties of 3% for the mean and 7% for the standard deviation of the fluctuations of *h*, given the spatial resolution of the measurements of 0.025 mm/pixel.

The measurement of the velocity of the liquid at the instant of breakup, $U_{detaching}$, which appears in Eqs. (9) and (10) was obtained from analysis of time-dependent series of images of the liquid

jets close to the breakup region. Image processing quantifies the displacement of the ligament formed during the breakup of the liquid jet (see Fig. 3) and, since the time between images is known, $U_{detaching}$ can be evaluated. Since the temporal resolution is 1/20 ms and the spatial resolution is 0.025mm/ pixel, and random measurement errors remained, the overall measurement uncertainty of velocity $U_{detaching}$ is around 5%.

The gas jet velocity, U_{imp}, close to the impingement location, which is at a distance of 12 nozzle diameters from the nozzle exit, is estimated as 0.6 times the area-averaged nozzle exit velocity, based on the airflow rate and the nozzle exit cross sectional area, for each flow condition. This estimate is without the presence of the liquid jets, according to the empirical expression for the rate of mean velocity decay along the centerline of a jet proposed by Spalding (1979). This value was also confirmed by Pitot tube and Laser Doppler Anemometry velocity measurements, the latter obtained by introducing fine 'seeding' droplets in the gas flow.

The PDPA instrument is a standard TSI system, which measures simultaneously two velocity components and size of the stable droplets in the resulting spray. The detailed description of the optical setup and the characteristics of the PDPA system can be found in Xia et al. (2017). The characteristics of the transmitting and receiving optics of the PDPA system and the resulting droplet sizing characteristics are also summarized here in Table 1. It is noted that the PDPA probe volume is traversed across the whole area of a cross section of the spray to measure the droplet characteristics throughout the spray, which may be non-axisymmetric due to the jets impingement arrangement of the atomizer. This information is necessary for the quantification of the atomization efficiency, as will be discussed below.

Table 1 Optical characteristics and operating droplet size range of the PDPA system

Transmitting Optics		
Channel for velocity component	Channel 1	Channel 2
Wavelength (nm)	514.5	488
Focal length (mm)	500	500
Laser beam separation (mm)	20	20
Laser beam diameter (mm)	1.7	1.7
Beam expander (ratio)	2	2
Expanded beam separation (mm)	40	40
Expanded beam diameter (mm)	3.4	3.4
Fringe spacing (μm)	6.4364	6.1049
Beam waist diameter (μm)	96.34	91.37

Bragg cell frequency (MHz)	40	40
Receiving Optics		
RVC front lens focal length (mm)	500	
RVC back lens focal length (mm)	370	
Slit aperture (μm)	150	
Off-axis Angle (°)	30	
Droplet Sizing		
Scattering mechanism	Refraction	
Polarization angle	Perpendicular	
Refractive index of the droplet	1.33	
Droplet size range (μm)	0.6 - 251	

Water flow rates are monitored by two calibrated Omega water flow meters with 1% accuracy, while the air flow rate is metered using an Alicat mass flow meter with an accuracy of ±0.3% of reading +0.2% F.S. The atomizer assembly is fixed onto a three-dimensional computer-controlled traverse system with a positional accuracy of 0.01 mm, which can move the atomizer at different locations along three directions (X, Y and Z). The geometrical impingement point *O* is set as the reference point (0, 0, 0) of the XYZ coordinate system shown in Figs. 1 and 2.

The PDPA of the droplet size measurements is less than $1\%D_{max}+1\%D_{measurement}$, where D_{max} is the maximum droplet size measured by the PDPA for the current optical configuration and $D_{measurement}$ is the value of the diameter of the measured droplets, with a repeatability of 0.5%, while that of the droplet velocity measurements was below 2% with a repeatability of 0.05% Lai et al. (2013). The overall uncertainties of the droplet Sauter mean diameter and mean velocity are estimated to be ±4% and ±1% respectively, including statistical uncertainties of 2% and 1% for size and mean velocity respectively, based on 10,000 samples for each measurement. The droplet volumetric flux, defined as the rate of liquid volume, carried by the droplets, crossing a unit area in the spray was also measured using the PDPA system, which is presented in this paper normalized by the maximum centerline value for each condition. The uncertainty of the volume flux was found to be less than 10% (Hardalupas et al. 1994) or rather around 5% (Sommerfeld and Qiu 1995), of the measured value for dilute sprays. However, the locally measured volume flux must be corrected for the local validation rate of the PDPA instrument at different locations in the spray. Table 2 shows the results for the absolute value of the measured liquid flowrate after integrating the measured radial distribution of volume flux in the spray, which is up to 30% lower than the supplied liquid volume flowrate and varies for

different operating conditions. This difference is caused by droplets crossing the measurement volume, but not generating signals that are validated by the PDPA software, either due to low signal-to-noise ratio or due to the light scattering characteristics that do not satisfy the validation criteria of the PDPA software. In addition, the sprays become quite dilute at the edge and, for some flow conditions, no measurements were obtained at these points, which leads to some loss of mass. When the validation rate of the instrument, which varies between around 10% and 30% for different locations and operating conditions, is considered to correct the measured liquid volume flow rates of Table 2, the remaining uncertainty for the normalized liquid volume flux is around ±5%. It is noted that the PDPA can measure the droplet sizes more accurately than alternative methods, i.e. laser diffraction or imaging, (for example Cossali and Hardalupas (1992) and discussion in that paper) used previously for quantification of the atomization efficiency.

Table 2 Measured and integrated volume flow rate from volume flux profiles

	Measured Q_L(ml/min)	150	200	250	300
2θ = 90°	Z=75mm	126.2	177.6	217.8	236.7
	Z=45mm			178.6	
	Z=105mm			192.2	
2θ = 60°				205.8	
2θ = 120°				254.2	

(The volume flux is converted to the unit of ml/min by multiplying the element area (5×5 mm^2))

Several parameters have been used in the literature to scale the atomization characteristics of airblast atomizers, including Air-to-Liquid Momentum Flux Ratio (ALMFR), Air-to-Liquid Momentum Ratio (ALMR), Air-to-Liquid mass flowrate Ratio (ALR), Weber number and liquid jet Reynolds number (Eroglu et al. 1991, Lasheras and Hopfinger 2000, Engelbert et al. 1995). These are defined for the current configuration as:

$$ALMFR = \rho_G U_{imp}^2 / 2\rho_L U_L^2 \quad (3)$$

$$ALMR = \dot{m}_G U_{imp} / \dot{m}_L U_L \quad (4)$$

$$ALR = \dot{m}_G / \dot{m}_L \quad (5)$$

$$We = \rho_G \left(U_G - U_L\right)^2 D_L / \sigma_L \quad (6)$$

$$\mathrm{Re} = \rho_L D_L U_L / \mu_L \qquad (7)$$

It has been shown by Engelbert et al. (1995) that the Weber number cannot scale the droplet sizes in the resulting sprays and, therefore, ALMFR and ALMR are mainly used to scale the results. However, we also provide the corresponding value of the Weber number in Table 3, which summarizes the operating conditions used for the current study. It is noted that the mass flowrate of the liquid in the definition of the ALMR is the total mass flowrate of the liquid supplied through the two liquid jets.

Table 3 Parameters of the experimental conditions for spray characterization

Parameters for measurements of breakup characteristics L and h								
Q_L(ml/min)	$\dot{m}_G$(g/min)	2θ		ALMR	ALMFR	ALR(×10^2)	Re	We
100	4.4	90	120	0.894	0.252	4.41	1541	31.57
100	6.75	90	120	2.089	0.585	6.75	1541	74.78
100	13.5	90	120	8.417	2.377	13.5	1541	309.60
100	27	90	120	33.667	9.508	27.0	1541	1250.47
Parameters for measurements of droplet size, velocity and volume flux								
Q_L	$\dot{m}_G$	2θ		ALMR	ALMFR	ALR	Re	We
100	13.5	90		14.03	2.377	0.135	1541	309.60
150	13.5	90		6.24	0.380	0.090	2311	306.59
200	13.5	90		3.51	0.264	0.068	3083	303.69
250	13.5	90		2.24	0.194	0.054	3853	300.62

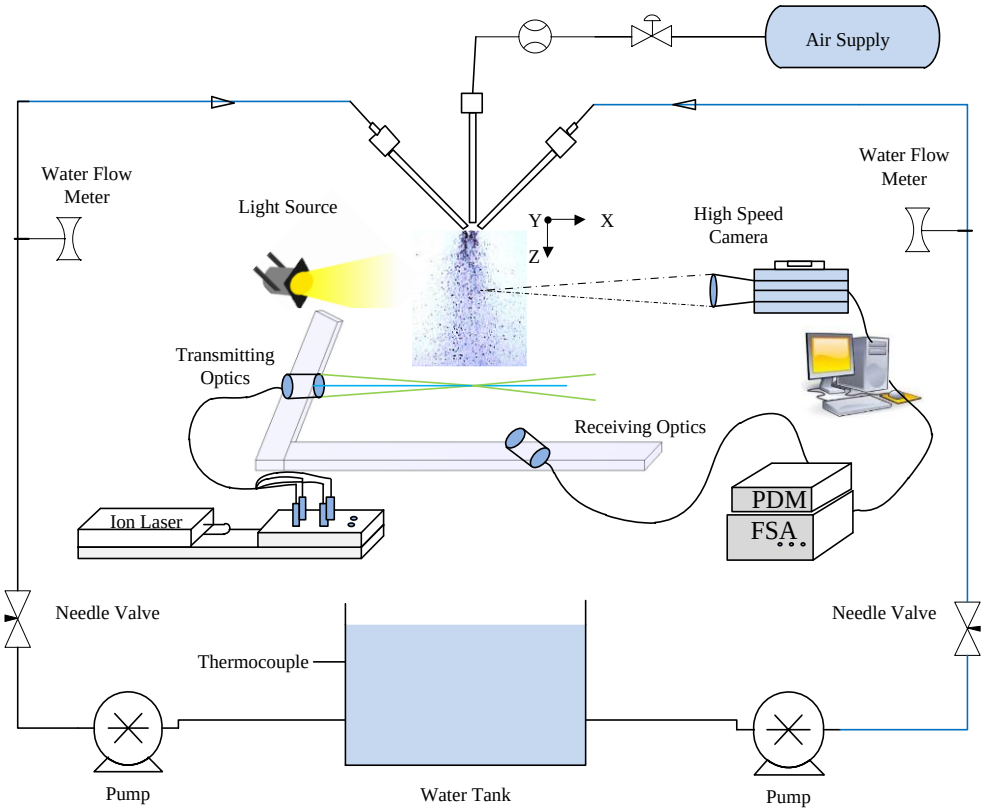
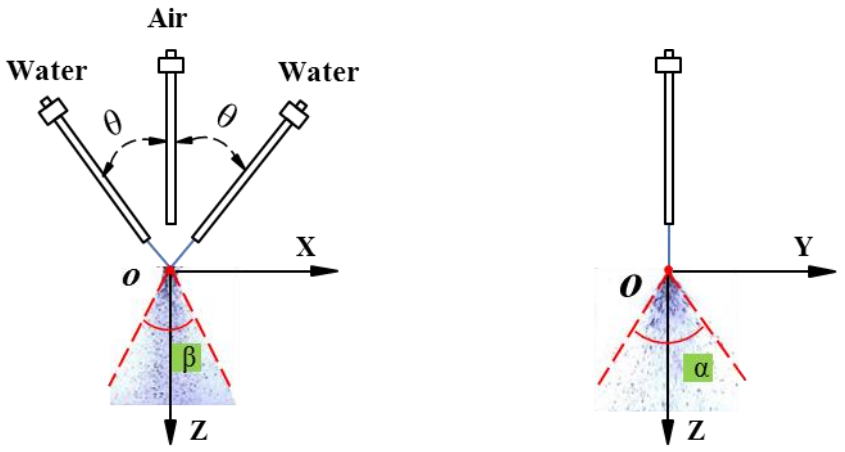


Fig.1. Schematic of experimental setup. PDM represents the control module of the Photodetectors and FSA the signal processor of the PDPA system.



(a) Side View (S.V.) **(b) Front view (F.V.)**

Fig.2. Schematic of the injector geometry, coordinate system and measured spray angles (a) side view (S.V.) spray angle β (in plane X-Z); (b) front view (F.V.) spray angle α (in plane Y-Z). (Pre-lengths for water jets are 10mm and air jet 12 mm)

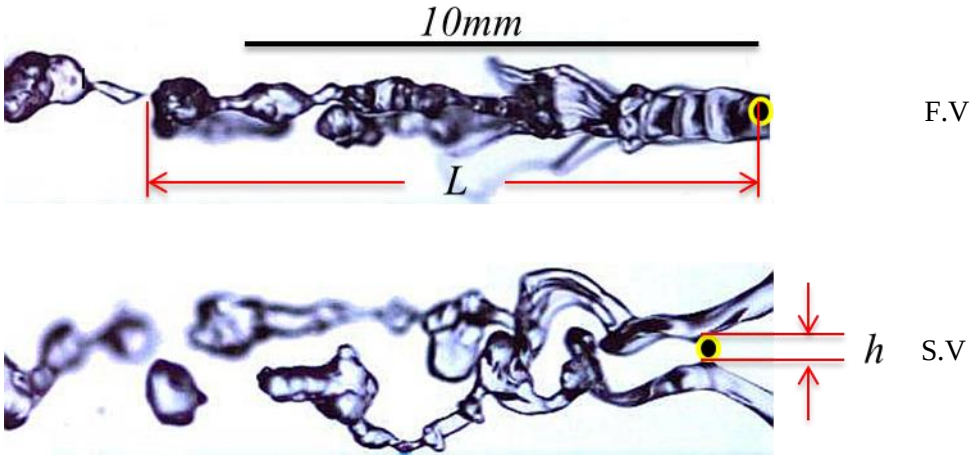
3. Results and discussion

Water jet breakup length L, the separation distance between the two intact water jets h at the geometrical impingement point, the velocity of the liquid fragments at the breakup location $U_{\text{detaching}}$ and the spray angles, as shown in Fig. 2 are evaluated from the captured images using high speed photography. Local and spatially-averaged SMD of the liquid droplets together with their velocities and liquid volume flux are measured with PDPA in the resulting sprays. Energy transfer between the liquid and air jets is quantified, for the first time, in terms of kinetic energy transfer from the air to the liquid jets up to the breakup location. Finally, we discuss and extend the energy transfer analyses in relation to the trends and values of the atomization efficiency, according to Lefebvre (1992) and Pizziol et al. (2018), to the current atomizers. The liquid flowrate $\dot{m}_L$ in this study refers to the sum of the flowrates of the two liquid jets.

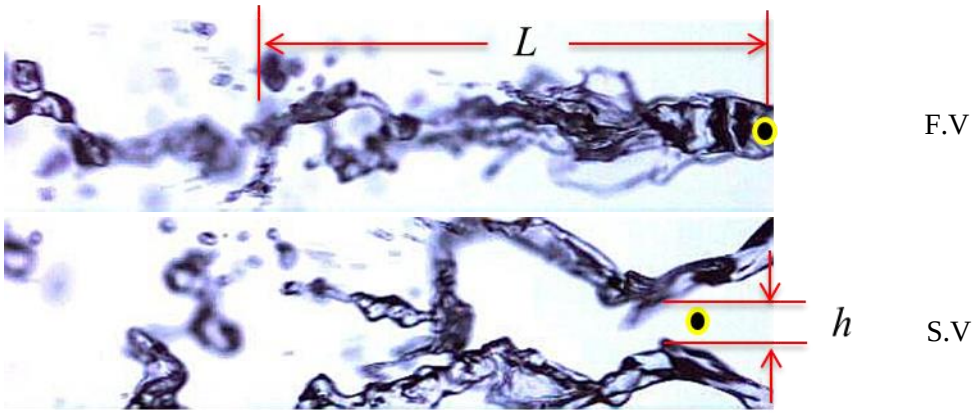
3.1. Liquid jet breakup length *L* and water jet separation distance *h*

The breakup length of the liquid jets is considered here due to its important role in primary atomization and in developing computational models to predict spray behaviors. As shown in Fig. 3, the breakup length of a water jet L is defined as the distance from the geometric impingement point to the position, where the liquid column becomes discontinuous. It is noted that the length of the liquid jet, upstream of the geometric impingement point and up to the nozzle exit, is 10 mm and, for the examined conditions, the liquid jet remains intact in this region. Figure 3 provides two views of the breakup region for a few operating conditions and shows the asymmetry of the atomization process that affects the shape of the cross sectional area and the level of asymmetry of the downstream sprays. Figure 3 also demonstrates qualitatively that the breakup length L decreases as the air flowrate increases, as Xia et al. (2017) also demonstrated.

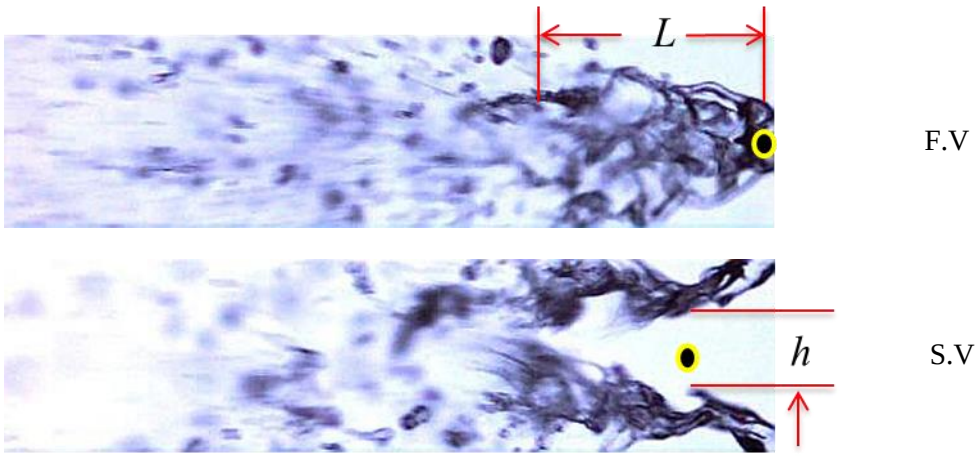
In addition, the instantaneous images of Fig. 3 show the behavior of the liquid jets near the geometric impingement point, marked by a ‘dot’ on the photographs. This is determined by the location where the axes of the two liquid jets cross the axis of the air jet. It is clear from the images that, when the air jet is present, the two liquid jets do not come into contact and there is a separation distance h that remains between the two liquid jets, which changes with the operating conditions. The air jet deflects the liquid jets before they reach the geometric impingement point and the interaction of the intact liquid jets does not occur at the impingement point. Therefore, despite the geometry of the atomizer, which implied the presence of impinging liquid jets, this did not happen when the air jet was present.



$\dot{m}_G$ = 4.4 g/min; *ALR*=4.41×10^{-2}, *ALMR*=0.894



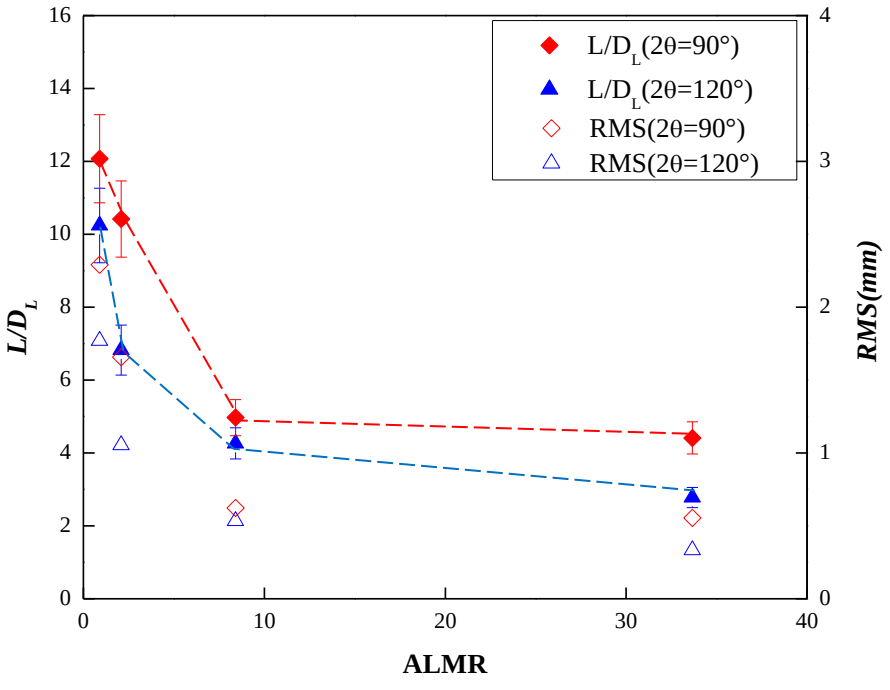
$\dot{m}_G$ = 6.75 g/min; *ALR*=6.76×10^{-3}, *ALMR*=2.089



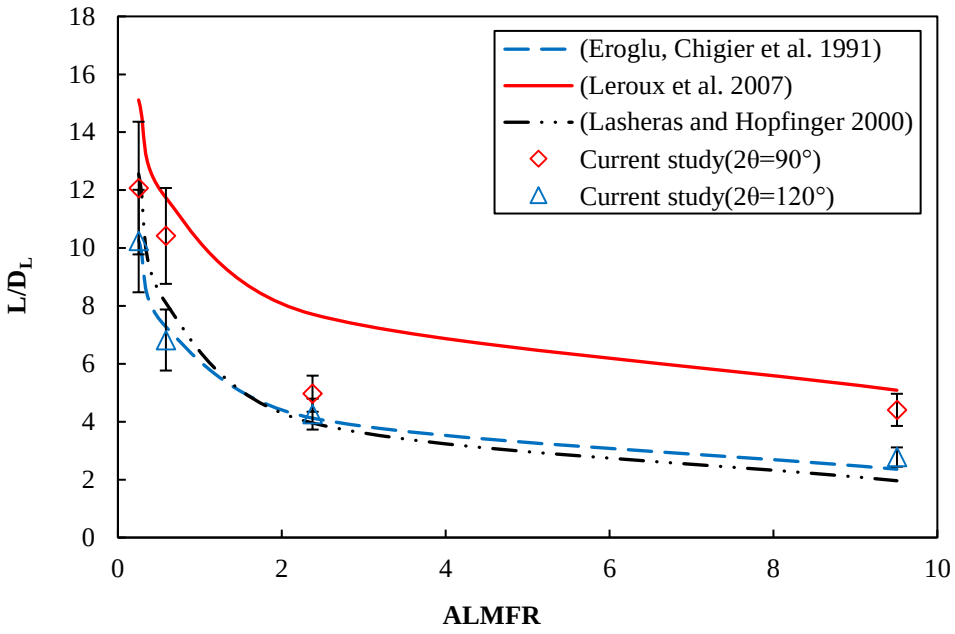
$\dot{m}_G$ = 13.5 g/min; *ALR*=13.52×10^{-3}, *ALMR*=8.417

Fig.3. Examples of liquid jet breakup length *L* and separation distance between the two liquid jets *h* close to the geometrical impingement point for different operating conditions for impingement angle 2θ = 90°. The dots on the images indicate the corresponding geometrical impingement locations for the considered atomizer. The views F.V. and S.V. are according to the definitions of Fig. 2. The liquid jets enter the images from the right hand side.

Figure 4(a) presents the breakup length, non-dimensionalized by the liquid jet nozzle diameter, as a function of ALMR defined in Eq. (4). This has the advantage of scaling the results better than the Weber number (*We* - Eq. (6)), since *We* cannot reveal the effect of liquid velocity change due to the small variation of the relative velocity difference between gas and liquid flows, when the liquid flowrate is varied. The air-to-liquid momentum flux ratio (ALMFR - defined in Eq. (3)), also has similar advantages over the Weber number and does not include the dimensions of the nozzles, see Engelbert et al. (1995), which is useful when attempting to scale the spray behavior of atomizer geometries with different dimensions. It can be observed in Fig. 4(a) that L/D_L decreases rapidly by around 2/3 of the initial value as ALMR increases from 1 to 9, and then the rate of breakup length decrease becomes low and the breakup length remained almost constant for ALMR > 9. The corresponding standard deviation (RMS) of the fluctuations of the breakup length in Fig. 4(a) follows a similar behavior with ALMR and the values are around 15% of the corresponding mean breakup length. The observed variability of the breakup length may be caused by local variations of the liquid and air jet flows.



(a)



(b)

Fig.4. (a)- Normalized mean breakup length L/D_L and RMS of its fluctuations as a function of ALMR for different liquid jet impingement angles, (b)- Comparison of L/D_L as a function of ALMFR for current atomizer geometry and other coaxial airblast atomizers. It is noted that ALMFR is selected to compare current results with previous research in the literature.

The increase of the impingement angle of the two liquid jets from 90° to 120° led to a reduction of the breakup length and the corresponding fluctuations by around 20%, which is due to the increased interaction between the injected air jet and liquid jets for the larger impingement angle and the behavior of the energy transfer from the air to the liquid streams, as quantified in Section 3.5.

Figure 4(b) displays a comparison of measured L/D_L from the current atomizer geometry with those obtained from previous correlations for coaxial airblast atomizers, such as from Eroglu et al. (1991), Lasheras and Hopfinger (2000) and Leroux et al. (2007). L/D_L is plotted as a function of ALMFR to assist the comparison with these previously proposed correlations. Generally, all correlations follow the same trend, namely L/D_L decreases sharply for low values of ALMFR and then the breakup length tends towards a near asymptotic value beyond ALMFR = 2, which coincides with the condition that the air jet separates fully the liquid jets and the direct interaction of the liquid jets is reduced. It is interesting to see such a good agreement between the breakup lengths of the liquid jets in a coaxial airblast atomizer, where the liquid and air flows are nominally parallel, and the current impinging jet atomizer, where the liquid jets are strongly inclined relative to the air flow. This demonstrates that the physics of the liquid

jet breakup process is not strongly affected by the air-liquid jet impingement angle and section 3.5 that presents the energy transferred from the air to the liquid jet upstream of the breakup location for different impingement angles will explain this observation.

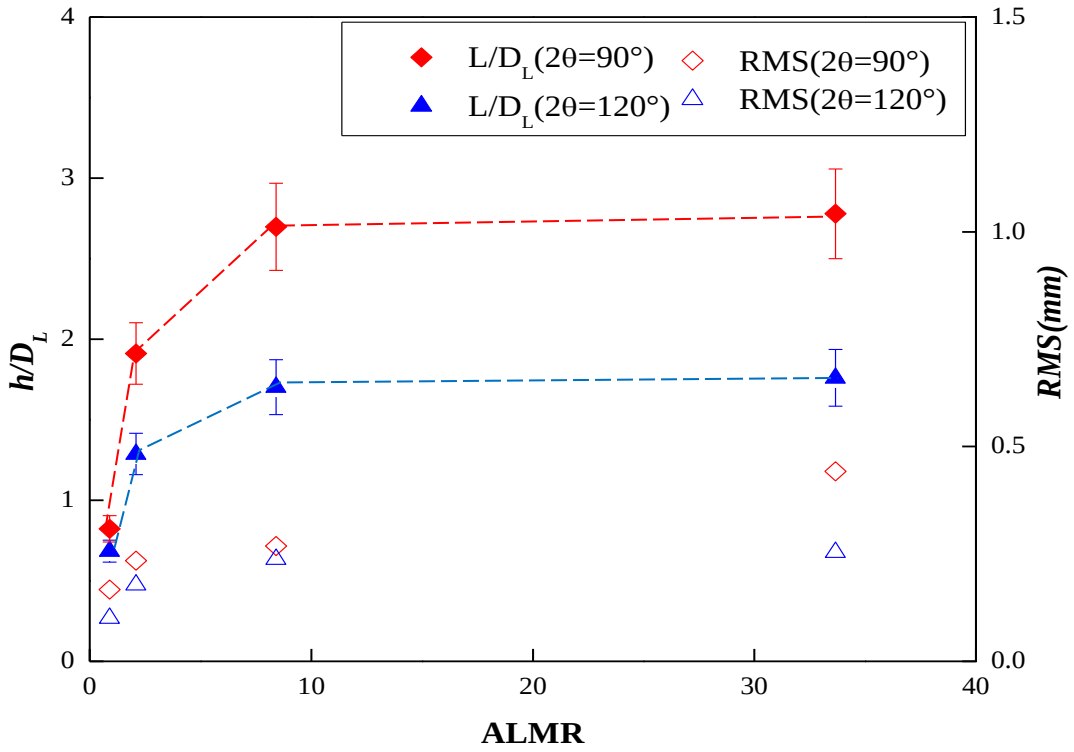


Fig.5. Mean liquid jets separation distance *h* (close to the geometrical impingement point) and RMS of its fluctuations as a function of ALMR for different liquid jet impingement angles.

Figure 3 demonstrated that the liquid jets do not come into contact. As shown in Fig. 5, the mean separation distance *h* between the two liquid jets close to the geometrical impingement point, normalized by the liquid jet diameter, first increases with increasing ALMR and then becomes constant beyond a value of ALMR of 9. The RMS of the fluctuations of the separation distance *h* also increases with ALMR in the region of the rapid change of h/D_L. The magnitude of the fluctuations is between 20 and 30% of the corresponding mean value for all reported conditions. This suggests that the distance between the two liquid streams influences the transfer of energy from the air to the liquid flow and, when h/D_L becomes larger, the interaction happens between each liquid jet and the edges of the air jet. This explains partly the behavior of the breakup length L/D_L in Fig. 4(a), which remains almost constant for ALMR > 9.

Both the RMS of the fluctuations of L/D_L (Fig. 4(a)) and h/D_L (Fig. 5) are a little larger for the liquid jet impingement angle of 90° than for 120°, suggesting that the instabilities of the flow interaction between the air jet and the liquid jets are larger for $2\theta = 90°$. Besides, both L/D_L and

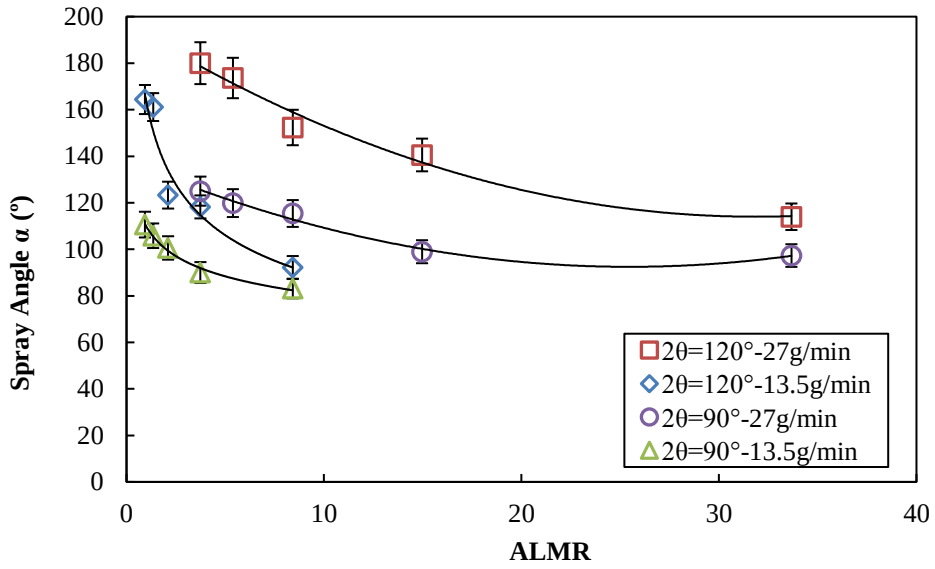
h/D_L decrease with increasing impinging angle. However, the effect remains small relative to the large change of the impinging angle, which is expected from the similar behavior of the current results and those of coaxial airblast atomizers in Fig. 4(b), since the coaxial atomizers represent the extreme condition of zero impingement angle between the air and liquid jets.

3.2. Spray angles (front and side views)

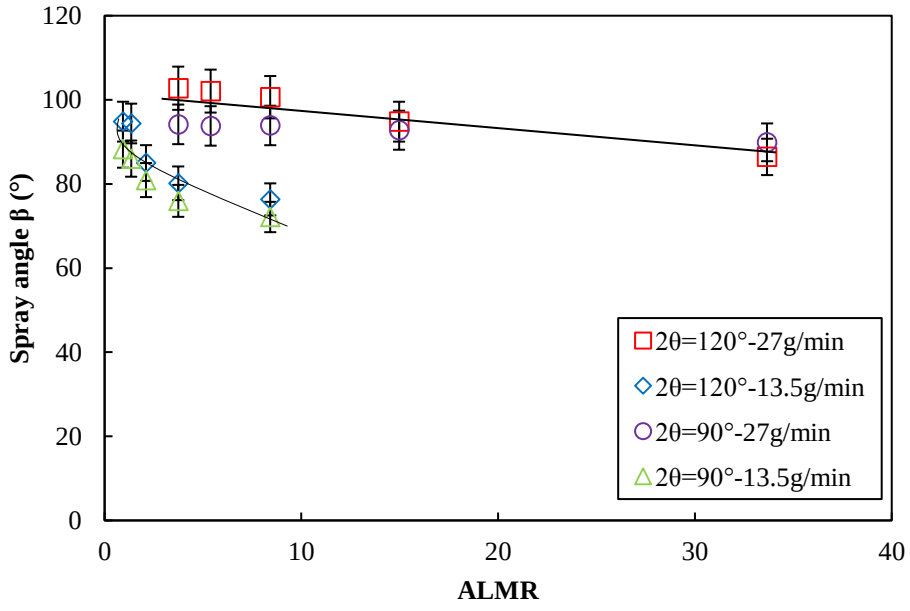
Spray angle is defined as the angle between the two boundaries of the region occupied by the water mist generated from the impinging jets atomization. Spray angles are quantified at two different planes (Y-Z and X-Z – see Fig. 2 for definition) of the spray, using Image J software (Collins 2007, Schneider et al. 2012). The mean spray angle is obtained by locating the geometrical impinging point and one point located 15 mm downstream the impingement point of Fig. 2 on the averaged spray image obtained from 400 instantaneous recordings.

Figure 6 presents the two spray angles as a function of ALMR for two air mass flow rates and impingement angles. Figure 6(a) shows that the spray angle α of Fig. 2 decreases with ALMR and tends towards a constant value as ALMR increases beyond 9 (for an air flow of 27 g/min), which is in agreement with the variations of the breakup length L and separation distance h of Fig. 4 and 5 respectively. No evident scaling of the spray angle α with ALRM can be observed, but larger impingement angles lead to larger α. This can be understood since the Y-Z plane coincides with the liquid membrane formed by the impingement of the two liquid jets in the absence of the air jet and the spatial extent of the membrane on this plane is strongly influenced by the impingement angle, see (Inoue et al. 2013, Xia et al. 2017). Fig. 6(b) presents the spray angle β of Fig. 2, which is on X-Z plane. One can notice that angle β decreases slowly with ALMR and almost linearly for an air flow of 27 g/min, whereas for the lower air flow of 13.5 g/min the angle decreases non-linearly. The results suggest that the spray angle β scales with ALMR with air mass flow as a parameter and that it is not sensitive to the liquid jets impingement angle.

Therefore, the characteristics of the breakup region demonstrated the importance of the interaction of the liquid jets with the air jet and the impact of the liquid breakup on the spray angle. The next section examines the shape of the spatial distribution of the spray droplets and their corresponding droplet characteristics.



(a) Spray angle α



(b) Spray angle β

Fig.6. Spray angles (a) α on Y-Z plane and (b) β on X-Z plane, defined in Fig. 2, as a function of ALMR for two air flowrates and two liquid jets impingement angles. Lines are added on the graphs for visual aid only.

3.3. Planar distributions of droplet SMD, velocity and normalized liquid volume flux

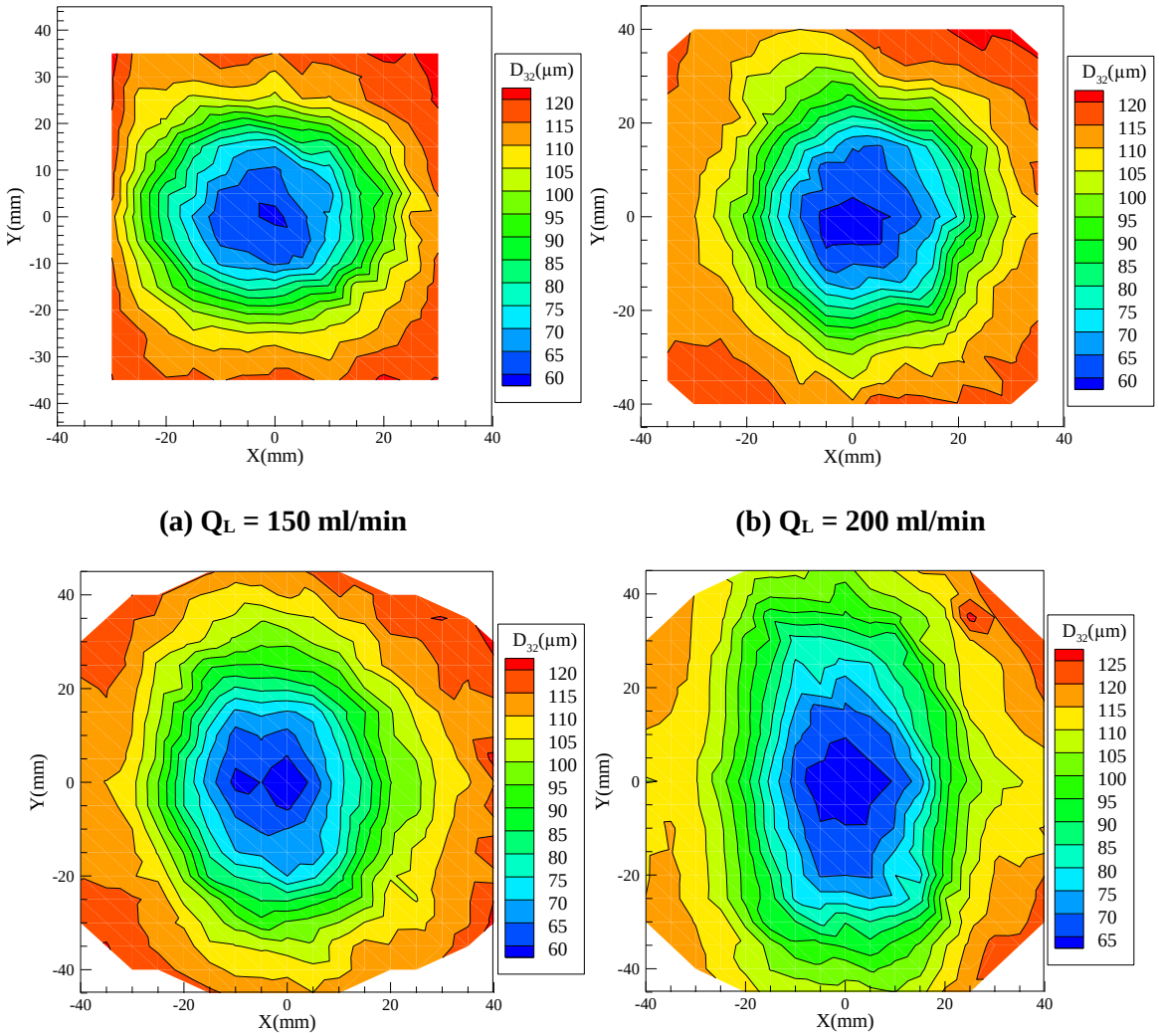
The results examine the effects of the water flowrate and liquid jet impingement angle on the spatial distribution of the droplet SMD, droplet velocity and normalized volume flux in a plane through the spray at an axial location Z = 75 mm. Contour plots of the above variables are

plotted, which are generated from the obtained measurements on a grid across the selected horizontal plane at Z = 75 mm that consisted of around 280 grid points. This grid resolution was found to be sufficient to resolve accurately the variation of the measured parameters across the plane. The horizontal plane at Z = 75 mm was selected because the atomization is complete at this distance and the spray droplets remain spherical, as reported by Xia et al. (2017), which ensures the accuracy of the PDPA measurements. This axial distance has a minimum SMD at the central region and remains close enough to the geometrical impingement point to ensure that the spray characteristics are captured before they are modified through interaction with the surrounding air flow further downstream (Xia et al. 2017). The characterization of the droplet characteristics across the full plane is due to the resulting non-axisymmetric downstream sprays due to the impinging jet atomization process that was demonstrated by the images of Fig. 3 and the spray angle results of Fig. 6. In this way, the characteristics of all droplets that are present in the downstream sprays are considered, which is important for the accurate quantification of the atomization efficiency.

Effect of water flowrate

The effect of water flowrate on the spatial distribution of droplet size, velocity and normalized liquid volume flux is investigated by performing measurements across the X-Y plane at axial distance Z = 75 mm for constant air flowrate of $\dot{m}_G$= 13.5 g/min and water volume flowrates Q_L = 150, 200, 250, 300 ml/min. As shown in Fig. 7, the spray spreads over a wider region with increasing water flow rates, though the minimum and maximum values of SMD remain surprisingly almost constant at about 60 μm and 120 μm respectively. This observation is discussed in terms of the energy transferred from the air to the liquid flow in Section 3.5.

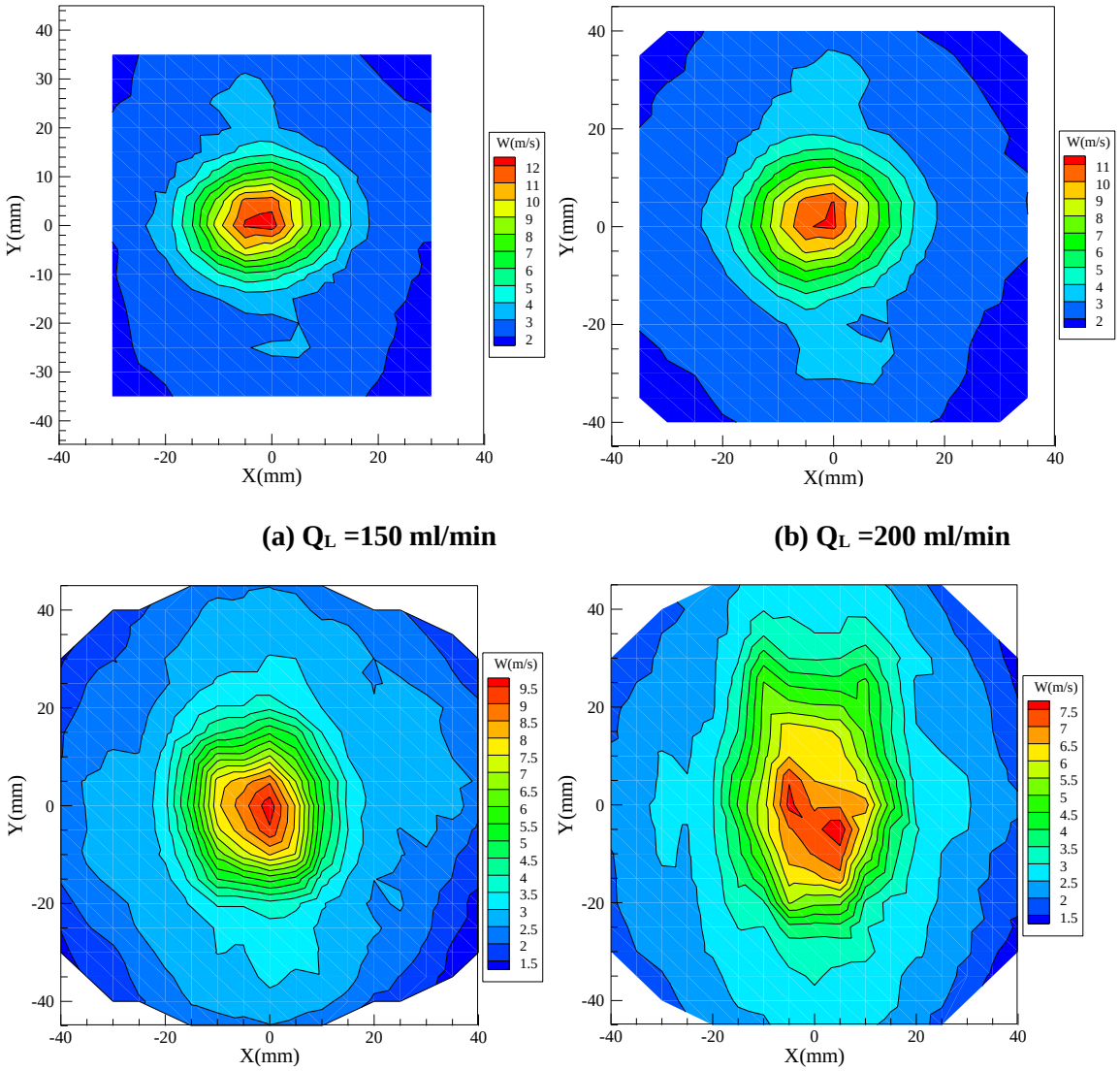
For water flowrate lower than 200 ml/min, the spray spatial distribution is nearly axisymmetric with small droplets existing in the central region of the spray, where the air jet shearing effects are most prominent, and larger droplets being present at the outer region. However, as shown in Fig. 7(c) and (d) for water volume flowrates Q_L = 250 and 300 ml/min, though SMD increases in a symmetric manner from the spray center in both X and Y directions, the contours indicate sprays with elongated region of smaller droplets along the Y-direction due to the augmented liquid jets impingement interaction with the air flow.



(a) Q_L = 150 ml/min **(b) Q_L = 200 ml/min**

(c) Q_L = 250 ml/min **(d) Q_L = 300 ml/min**

Fig.7. Spatial distribution of droplet Sauter Mean Diameter, SMD, along the X-Y plane at axial distance Z = 75 mm. Operating condition corresponds to liquid jets impingement angle 2θ = 90° and air mass flowrate $\dot{m}_G$ = 13.5 g/min for different liquid volume flowrates. (a) Q_L = 150 ml/min, ALMR=3.741; (b) Q_L = 200 ml/min, ALMR=2.104; (c) Q_L = 250 ml/min, ALMR=1.347; (d) Q_L = 300 ml/min, ALMR=0.935. Note that the water flowrate Q_L is the sum of the supply to the two liquid jets.



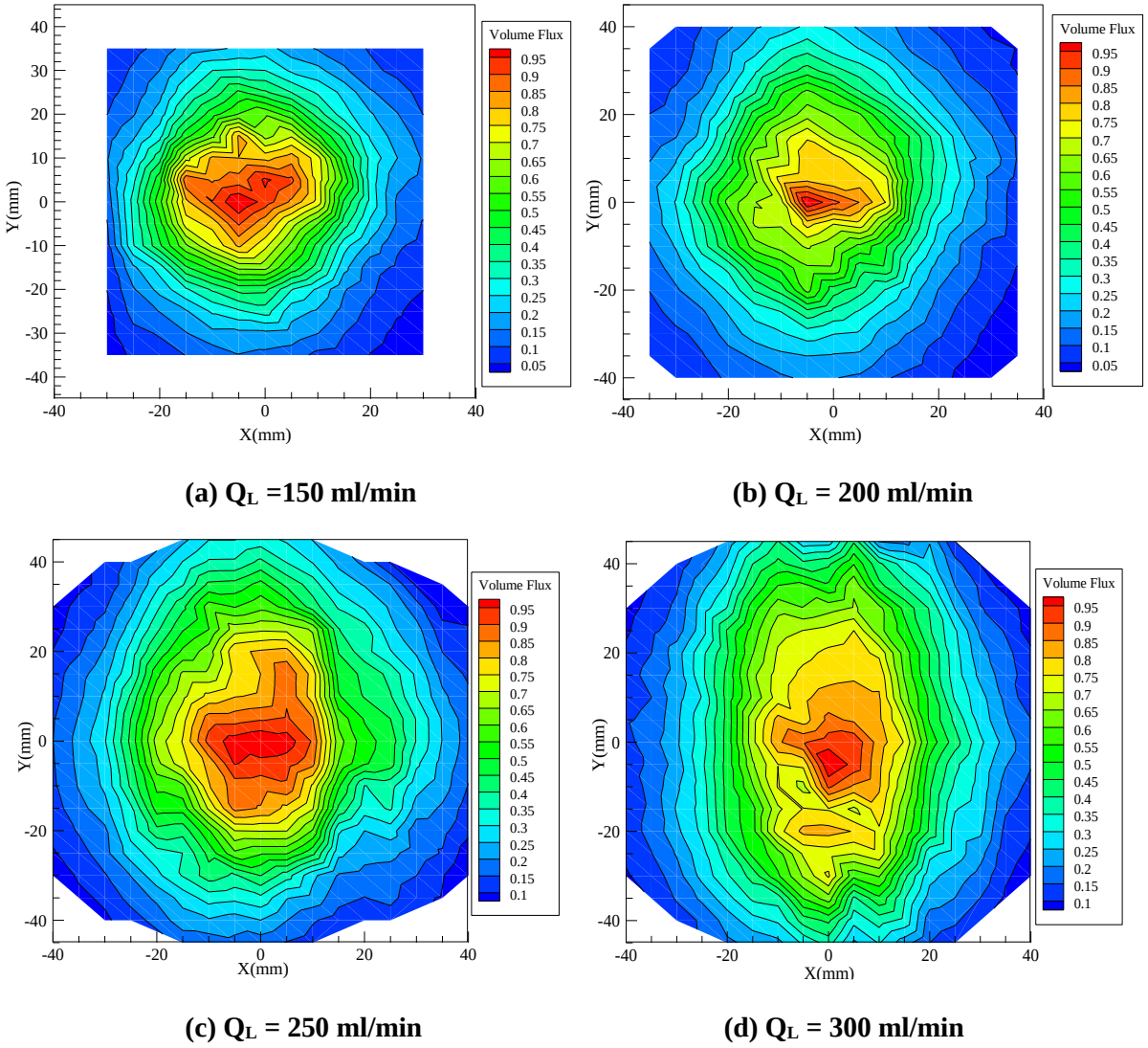
(a) Q_L =150 ml/min **(b) Q_L =200 ml/min**

(c) Q_L =250 ml/min **(d) Q_L =300 ml/min**

Fig. 8. Spatial distribution of droplet mean axial velocity, W, along the X-Y plane at axial distance Z = 75 mm. Operating condition corresponds to liquid jets impingement angle 2θ = 90° and air mass flowrate $\dot{m}_G$ = 13.5 g/min for different liquid volume flowrates. (a) Q_L = 150 ml/min, ALMR=3.741; (b) Q_L = 200 ml/min, ALMR=2.104; (c) Q_L = 250 ml/min, ALMR=1.347; (d) Q_L = 300 ml/min, ALMR=0.935. Note that the water flowrate Q_L is the sum of the supply to the two liquid jets.

The spatial distribution of the droplet mean axial velocity, W, along the Z direction is presented in Fig. 8 for liquid jets impingement angle 2θ = 90°, air flowrate $\dot{m}_G$ = 13.5 g/min and different liquid flowrates. Figure 8 shows that a central region with maximum velocity is present, where the direct momentum exchange between the air and water droplets mainly occurs. This region coincides with the presence of the smallest droplet sizes, which respond faster to the local air flow characteristics due to the fact that smaller droplets have smaller inertia. The droplet

velocity decreases at large radial distances from the centre, where the large droplet sizes are present, to reach minimum values at the edge of the spray. The value of the maximum velocity decreases from 12 m/s at Q_L = 150 ml/min to 7.5 m/s at Q_L = 300 ml/min due to the increased liquid mass present in the central region, which needs to be atomized and accelerated. Similar to the SMD distributions of Fig. 7, the velocity contours loose their axisymmetry for larger water flowrates and become elongated in the Y direction.



(a) Q_L =150 ml/min **(b) Q_L = 200 ml/min**

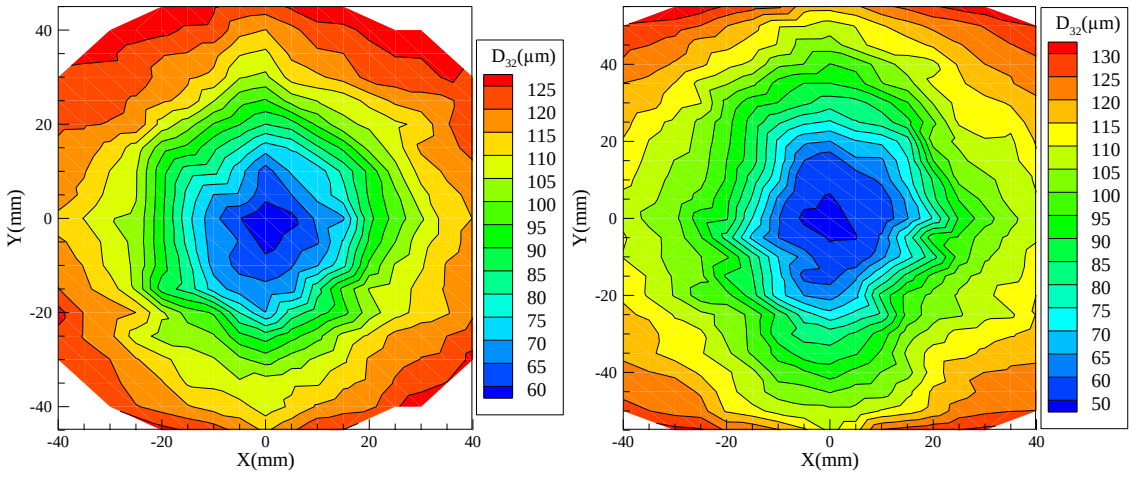
(c) Q_L = 250 ml/min **(d) Q_L = 300 ml/min**

Fig.9. Spatial distribution of normalized liquid volume flux along the X-Y plane at axial distance Z = 75 mm. Operating condition corresponds to liquid jets impingement angle 2θ = 90° and air mass flowrate $\dot{m}_G$ = 13.5 g/min for different liquid volume flowrates. (a) Q_L = 150 ml/min, ALMR=3.741; (b) Q_L = 200 ml/min, ALMR=2.104; (c) Q_L = 250 ml/min, ALMR=1.347; (d) Q_L = 300 ml/min, ALMR=0.935. Note that the water flowrate Q_L is the sum of the supply to the two liquid jets.

Figure 9 presents the spatial distribution of the liquid volume flux carried by the droplets, normalised by the maximum centreline value for each condition, along the plane X-Y at an axial distance Z of 75mm in the spray for operating conditions of liquid jets impingement angle 2θ = 90° and air flowrate $\dot{m}_G$ = 13.5 g/min for different liquid flowrates. Figure 11 shows that the increase of water flowrates leads to a wider spray cross section, which is expected from the increased spray angle at the impingement region, as quantified in Fig. 6. In addition, similar to SMD and mean axial droplet velocity contours, for Q_L > 250 ml/min, the normalised liquid volume flux distribution becomes elongated along the Y axis, as the spray becomes non-axisymmetric.

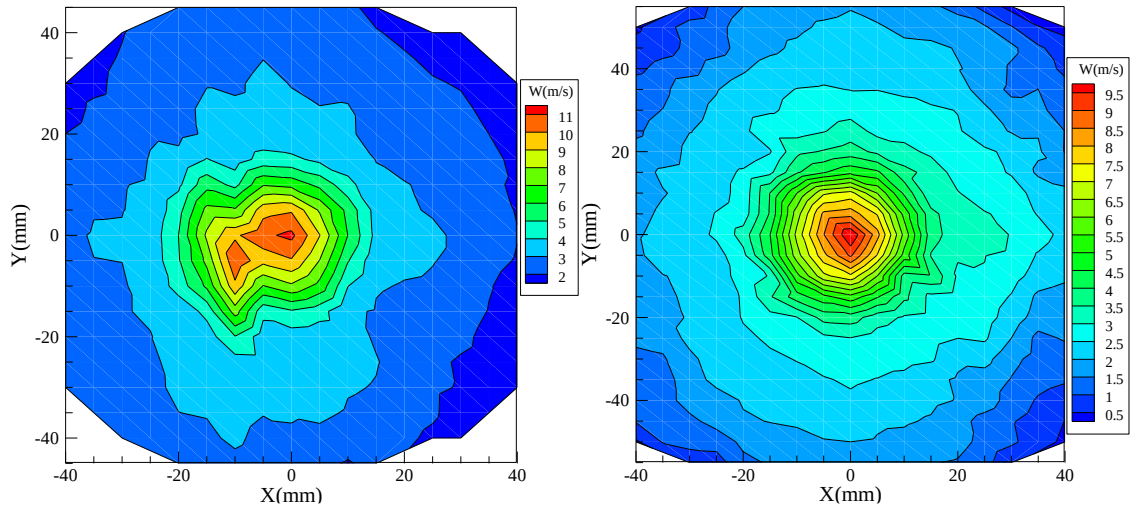
Effect of liquid jet impingement angle

The effect of the liquid jets impingement angle on the spray characteristics is evaluated in terms of SMD, mean axial droplet velocity *W* and normalized liquid volume flux spatial distributions along the plane X-Y at Z = 75 mm, for Q_L = 250 ml/min and air flowrate $\dot{m}_G$= 13.5 g/min for three cases of 2θ = 60°, 90° and 120°. The spatial distributions of the three quantities for 2θ = 90° have already been presented in Figs. 7-9. It is found that, even though the overall distributions are similar for the three cases, the spray is wider for impingement angle 2θ = 120° (Fig. 10(a)) and the droplets are relatively smaller than for the other two smaller impingement angle cases at the corresponding locations.



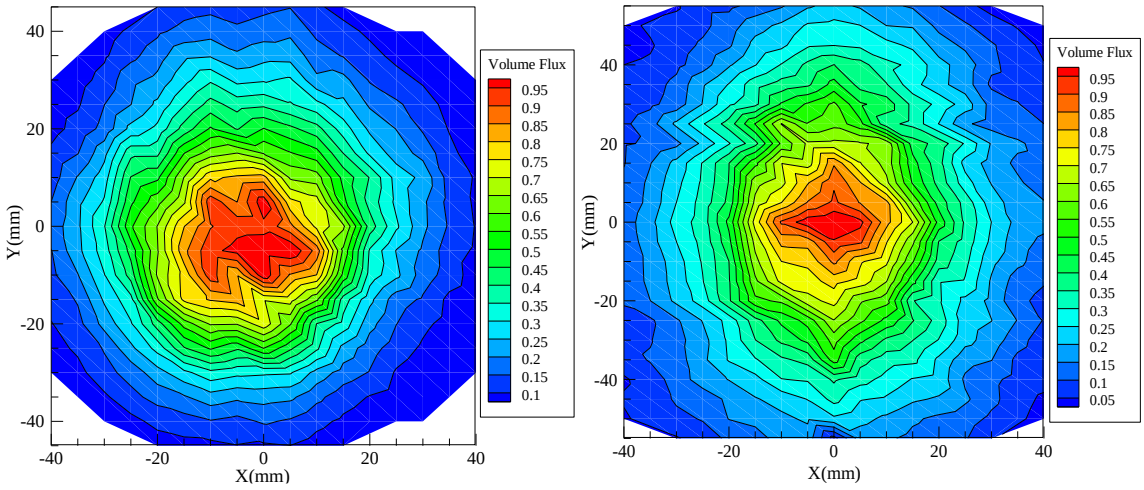
2θ = 60° **2θ = 120°**

(a)



2θ = 60° **2θ = 120°**

(b)



2θ = 60° **2θ = 120°**

(c)

Fig.10. Spatial distribution of droplet (a)- Sauter Mean Diameter **(**SMD), (b)- droplet mean axial velocity, W, (c)- Spatial distribution of normalized liquid volume flux, along the X-Y plane at axial distance Z = 75 mm. Operating condition corresponds to liquid volume flowrate Q_L =250 ml/min and air mass flowrate $\dot{m}_G$ = 13.5 g/min (ALMR=1.347) for liquid jets impingement angle of 2θ = 60° and 2θ = 120°.

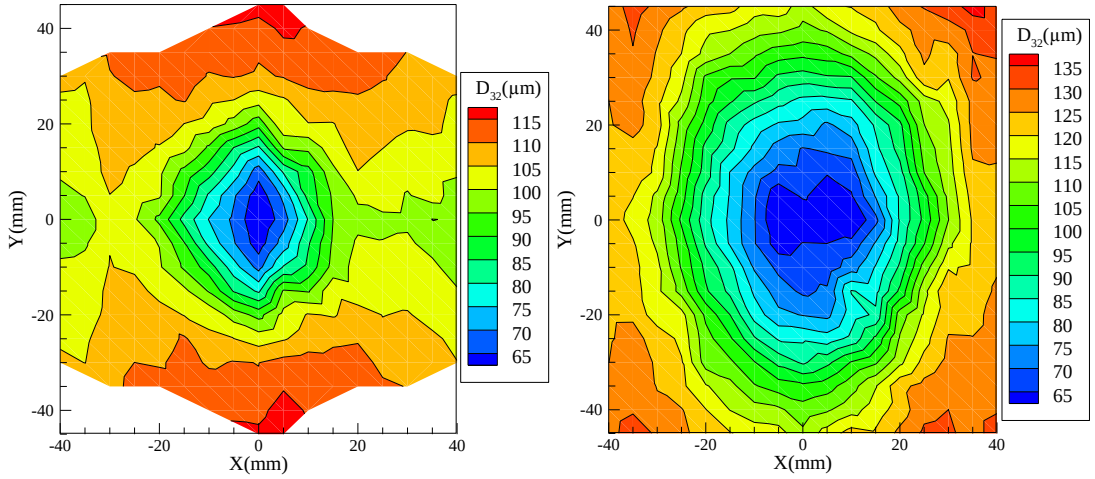
The mean droplet axial velocity is shown in Fig. 10(b) and it is larger for 2θ = 60°, since the axial velocity component of the droplet velocity is expected to be larger for conditions with smaller impinging angle.

The normalized axial liquid volume flux is presented in Fig. 10(c) and the changes with impingement angle follow the behavior of the spray angle presented in Fig.6. The main observation is that the spatial distribution becomes non-axisymmetric and elongated along the Y-direction for the larger liquid jets impingement angle, which suggests that the non-axisymmetric distribution of the spray starts at lower liquid flowrates for large impingement angles.

Variation of spray characteristics with axial position

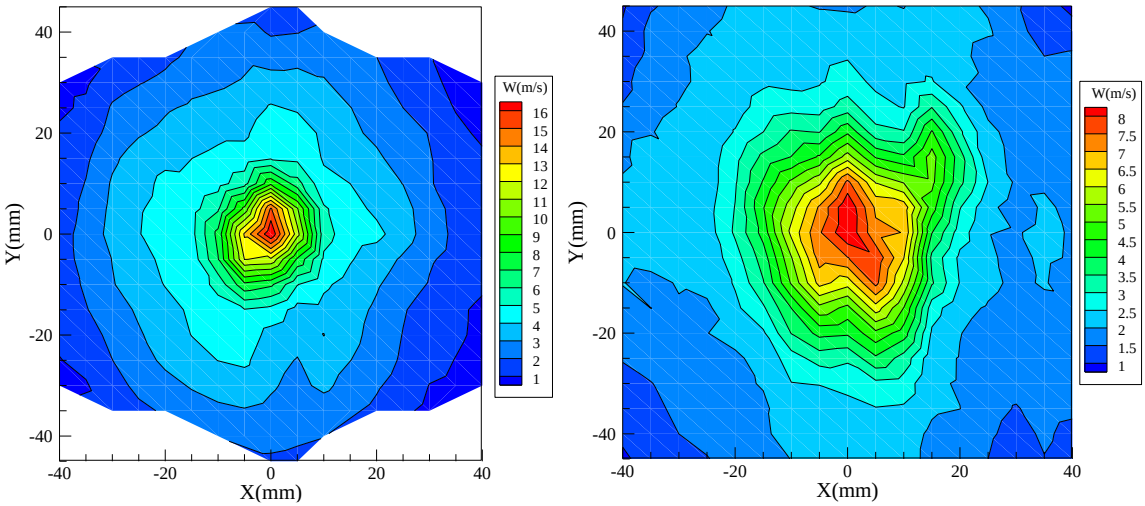
In order to study the variation of the SMD, droplet mean axial velocity and normalized liquid volume flux distributions along the vertical axis of the spray, measurements were obtained across X-Y planes at axial distances Z = 45, 75 and 105 mm for liquid jet impingement angle of 2θ = 90°, liquid volume flowrate Q_L =250 ml/min and air mass flowrate $\dot{m}_G$ = 13.5 g/min corresponding to ALMR = 1.347. The contour plots for axial location Z = 75 mm were presented in Figs. 7-9. Figure 11 presents the SMD, droplet mean axial velocity and normalized liquid volume flux spatial distributions respectively at axial locations Z = 45 and 105 mm. These figures and the corresponding graphs in Figs 7-9 show that, as the spray travels downstream from the nozzle exit, the cross stream area of the spray increases and the spatial distributions of SMD, droplet velocity W and normalized liquid volume flux are modified. Considering the minimum value of SMD of the droplets in the central region, it can be seen that it remains nearly constant at a value of around 65 μm over the considered axial distance. Following the work of Sallam et al. (2004) for a liquid jet subjected to an air stream, when shear break up takes place, as is the case for current flow conditions, the wavelengths of the instabilities at the liquid interface are of the order of $0.1D_L$. The size of these interface wavelengths was proposed to determine the diameter of the generated ligaments during breakup in this regime and hence scale the droplet SMD. The estimate of the size of the interface wavelengths for the current conditions is 69 μm, which is very close to the measured SMD of 65 μm in the central region of the spray. On the other hand, the maximum value of SMD at large radial distances from the centerline increases with increasing axial position from 115 to 135 μm. This is probably due to the faster radial dispersion of smaller droplets, which tend to follow the air flow well, while the large droplets follow straight trajectories, as demonstrated by flow visualization, which are not affected by the air flow. This is a direct proof of the fan spreading of large droplets. There may be some intermediate size droplets that are responding to turbulent flow structures, but these do not carry the majority of the liquid flowrate. As a consequence, at a radial position where SMD is maximum at the first axial station, the

droplet size distribution has a larger number of small droplets than further downstream. Small droplets gradually disperse away with increased axial distance, reducing the probability of small droplets in the droplet size distribution at the location of maximum SMD at larger axial distances, which leads to the observed increase of the SMD with axial distance.



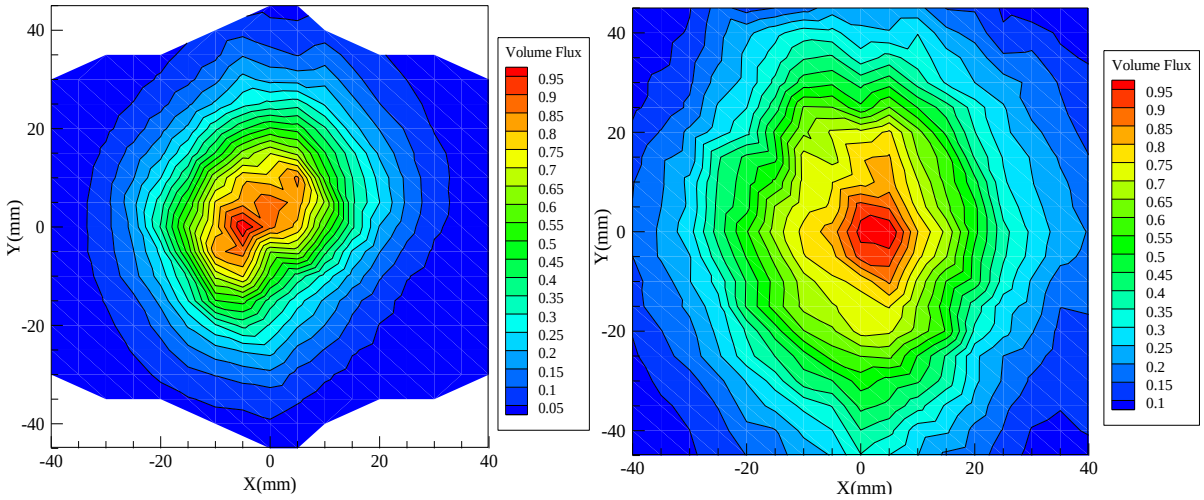
Z=45 mm **Z=105 mm**

(a)



Z = 45 mm **Z = 105 mm**

(b)



Z = 45 mm **Z = 105 mm**

(c)

Fig.11. Spatial distribution of (a)- droplet Sauter Mean Diameter, SMD, (b)- mean axial velocity, W, (c)- normalized liquid volume flux, along the X-Y plane at different axial distances in the spray (a) Z=45 mm; (b) Z=105 mm. Operating condition corresponds to liquid volume flowrate Q_L =250 ml/min, air mass flowrate $\dot{m}_G$ = 13.5 g/min (ALMR=1.347) for liquid jets impingement angle 2θ = 90°.

As shown in Fig. 11(b), the maximum mean axial droplet velocity at the central region of the spray decreases with downstream distance, as expected, because of drag and air jet expansion. The liquid volume flux distribution, normalized by the maximum value at the center of the spray, shown in Fig. 11(c), becomes wider with axial distance from Z = 45 mm to Z = 105 mm as a result of the fan-shaped spread of the spray from the impingement location, in agreement with the initial spray angle reported earlier. This is due to the limited response of the large droplets to the air flow turbulence. Since the large droplets carry most of the liquid volume in the spray, the spatial distribution of the liquid flux is mainly determined by the initial conditions of the formation of the large droplets, which follow the 'fan-spreading' behavior, as described in Hardalupas et al. (1989), and therefore maintain the original spray angle of the breakup region. The local volume flux in the central region becomes smaller with increasing distance from the spray impingement point, as the smaller droplets spread radially due to partial response to the air flow turbulence. However, the integral of the liquid volume flux over a cross section of the spray remains equal to the supplied liquid flowrate to the nozzle within ±5% after correcting the absolute values of the measured volume flux by the validation rate of the

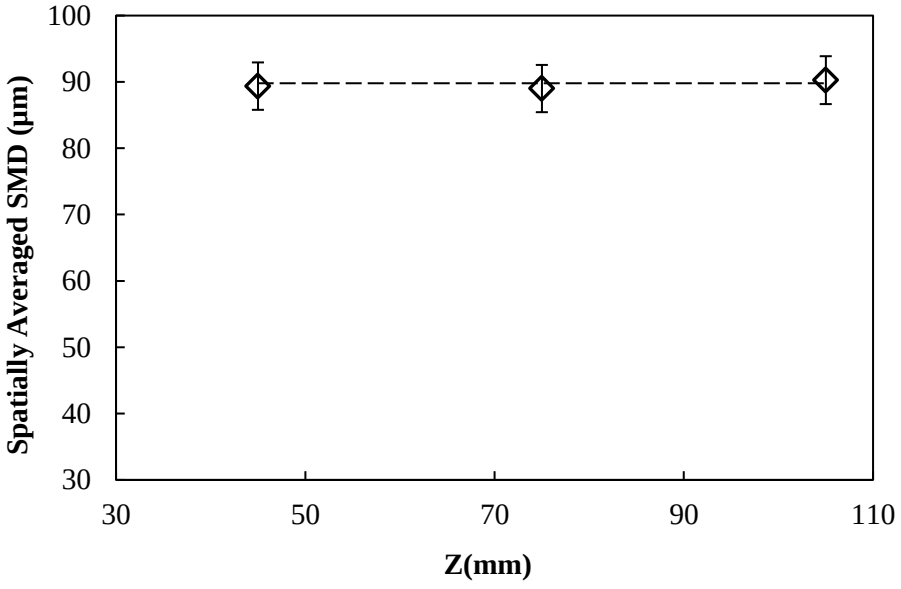
instrument, as discussed in Section 2. This has also been discussed by Hardalupas et al. (1994) and they showed that the uncertainty of this measurement was within 10% for their atomizer.

3.4. Spatially-averaged SMD and atomization quality

As can be seen from the difference between the spray angles obtained from front and side views, the resulting spray from the water-air impinging atomizer is not axisymmetric for a range of operating conditions. Consequently, radial profiles of local SMD in one direction may not be sufficient to quantity the atomization quality of the spray. This is a limitation of the approaches used from previous researchers in order to evaluate the atomisation quality and atomisation efficiency of the resulting sprays, as discussed in Section 1. Hence, in order to evaluate the atomization efficiency at different conditions independently of the spread rate of the droplets, which varies with droplet size, a weighted spatially averaged Sauter Mean Diameter is calculated. This is achieved by integrating the spatial distribution of the SMD weighted by the liquid volume flux over a cross section plane of the spray, as defined in Xia et al. (2018a).

$$\overline{SMD} = \frac{\int SMD(x,y)G(x,y)dxdy}{\int G(x,y)dxdy} \tag{8}$$

where SMD(x,y) is the local value of the measured Sauter Mean Diameter at point (x,y) of the spray, G(x,y) is the local volume flux of the droplets, measured by the PDPA across an axial plane at location Z, and $dxdy$ is the elemental area of the local section of the measurement grid through the spray.



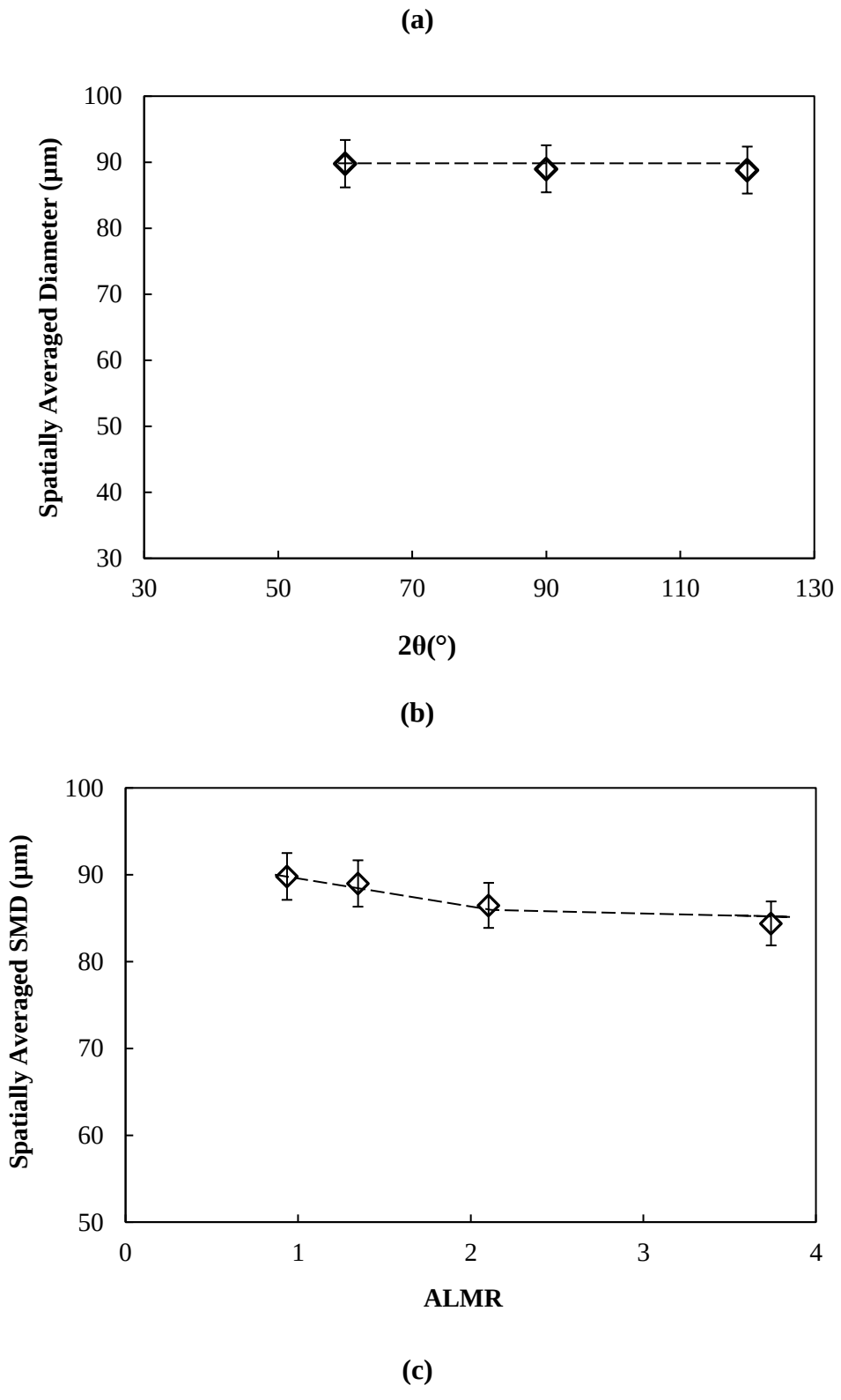


Fig.12. Spatially-averaged SMD, according to Eq. (8), inside the spray for different operating conditions. (a) At different axial distances from the atomizer for operating condition Q_L = 250 ml/min, $\dot{m}_G$ = 13.5 g/min, ALMR=1.347 and 2θ = 90°. (b) As a function of different liquid jets impinging angles for operating condition Q_L = 250 ml/min, $\dot{m}_G$ = 13.5 g/min, ALMR=1.347, measured at Z = 75 mm. (c) As a function of air-to-liquid momentum ratio, measured at Z = 75 mm for operating conditions of 2θ = 90° and $\dot{m}_G$ = 13.5 g/min and different liquid flowrates.

Figure 12(a) shows the spatially averaged SMD at three different axial positions under the same experimental conditions. The results show that there is no difference among the three positions, since the spatially averaged SMD remains constant at around 90 μm. Since the experiments were performed with water, droplet evaporation is negligible at atmospheric conditions. In addition, if the atomization process is complete, the droplet sizes in the spray do not change with axial distance. Inter-droplet collisions may also influence the spatial evolution of the droplet sizes in the spray. However, the sprays are relatively dilute to expect significant probability of collisions. In addition, the lack of change of the value of the spatially averaged SMD with axial distance for the same spray supports negligible number of collisions. It would be a large coincidence to obtain such a balance between new small droplet generation due to breakup and new large droplet generation due to coalescence during inter-droplet collisions, so that the resulting spatial distribution of droplet sizes lead to a spatially averaged SMD that remains constant with axial distance. Therefore, although different droplet sizes may disperse differently within the spray, the spatially-averaged SMD should not change. This expectation is confirmed by Fig. 12(a), which also demonstrates that local profiles of droplet sizes in the form of SMD in sprays, although necessary, are not sufficient to draw conclusions on the atomization quality and efficiency of the atomizer, since the selection of the appropriate local droplet mean diameter is not obvious. At the same time, the results of Fig. 12(a) indicate that a spatially-averaged SMD measured at just one single axial location is enough to characterize the atomization quality and efficiency. Although the SMD is presented here, it is possible to calculate other spatially averaged mean diameters. It is noted that the fact that the SMD remains constant with axial distance within the same spray demonstrates the low uncertainty of the reported PDPA measurements.

The effect of the liquid jets impingement angle on the spatially averaged SMD is presented in Fig. 12(b). The measurements were obtained at axial location Z = 75 mm for the same operating condition of Q_L = 250 ml/min and $\dot{m}_G$ = 13.5 g/min, ALMR = 1.347. Surprisingly, the spatially averaged SMD remains constant for different impingement angles, while the other conditions remain the same. This is an important finding, which demonstrates that the atomization quality of the resulting spray does not change with the jets impingement angle, which was not possible to conclude from the local values of the droplet SMD at the earlier sections. Since the energy input in this case is maintained constant and the spatially averaged SMD does not change with the change of the impingement angle, the atomization efficiency is not affected by the impingement angle. This is a novel result and demonstrates that the importance of the

impingement angle between air and liquid streams has no effect for the current atomizer and possibly very limited effect for other atomizer designs.

Fig. 12(c) shows the change of the spatially averaged SMD as a function of ALMR, measured at Z = 75 mm. The operating conditions of the atomizer were fixed to jet impingement angle $2\theta = 90°$ and air flowrate $\dot{m}_G$ = 13.5 g/min, while the liquid flowrate was changed leading to the observed changes of the ALMR. The following observation from Fig. 12(c) is surprising. The spatially-averaged SMD in the spray increases by about 5.6% as the liquid flowrate increases by a factor of around 3, leading to a decrease of the ALMR from 3.74 to 1. This suggests that the droplet sizes generated by the atomizer are increased with the increase of the liquid flowrate, which is a common observation for most atomizers. However, the increase of the liquid flowrate by a factor of 3 leads to significant increase of energy input to the atomizer, which leads to only a small deterioration of the atomization quality by 5.6%. This may support the assumption of Lefebvre (1992) that the energy of the air stream is important for the improvement of the atomization quality. Therefore, the exchange of energy between the air and liquid streams is very important for the atomization quality rather than the overall energy input.

This observation may be explained by the changes of the breakup process of the liquid jets with ALMR. The results of the previous section showed that the breakup length of the liquid jet *L* (Fig. 4) and the jet separation distance *h* of the two liquid jets close to the geometrical impingement point (Fig. 5) vary significantly for a range of ALMR between 1 and 3.74. Therefore, there is a significant change in the interaction between the air and water jets within this ALMR range, which limits the energy transfer between the air and liquid streams during the breakup process, which limits the ability to improve the atomization. The energy exchange between the air and liquid streams and the atomization efficiency are presented in section 3.5, where the consequences of the findings from Figure 12(c) will also be discussed.

3.5. Energy considerations and atomization efficiency

Figure 13 presents the Specific Kinetic Energy Increase (SKEI - defined in Eq. (9)) of the liquid jet at the point of breakup as a function of the ALMR. SKEI represents the extra energy that the liquid jet acquired from the air flow before its breakup.

$$SKEI = U^2_{\text{det}aching} - U^2_L \qquad (9)$$

where $U_{detaching}$ is the axial velocity of the liquid at the breakup position, which is defined in section 2 and U_L is the velocity of the liquid jet at the nozzle exit. It is noted that Eq. (9) assumes

that the liquid mass is conserved upstream of the breakup point, for example, no droplet stripping from the liquid interface occurs and ignores the loss of kinetic energy by the liquid to the surrounding air, since the liquid is slower that the surrounding air flow, and the rotational component of its kinetic energy, since the initial conditions of the air and the liquid flows do not include swirl and do not impart angular momentum to the flow.

Figure 13 shows that the specific kinetic energy transferred from the air jet to the liquid jets increases non-linearly by around 10 times for an increase of the ALMR by 10 times. The figure also shows a similar change for the liquid velocity at the breakup location, $U_{detaching}$, as expected. It is noted that the error bars in the figure represent the propagation error from the uncertainty caused by systematic and random errors in the velocity measurement. Close examination of Fig. 13 identifies two regions: the first, where SKEI increases steeply for ALMR values between 0 and 3, and thereafter, where SKEI increases with a different lower slope up to ALMR of 33. The results show that the transfer of energy from the air to the liquid stream is more efficient at low ALMR and less so for high values of ALMR. It should be noted that, for high values of ALMR, some small droplets, which carry small liquid mass, can be peeled off the surface of the water jet before its breakup, which results in a small mass loss from the liquid core that is not considered in Eq. (9). Consequently, the remaining mass of the water core tip can be accelerated to a higher velocity with the transferred energy from the air jet, which results in a larger increase of SKEI for high ALMR. Despite this uncertainty due to small liquid mass loss from the liquid core, the rate of change of SKEI for high values of ALMR is lower than for ALMR<3 and the above uncertainty does not affect the observed conclusions. When ALMR is less than 3, the air flowrate is low. So, for ALMR nearly 0, the local air and liquid velocities become similar or alternatively the liquid velocity is higher than the air velocity. The spray images, superimposed on Fig. 13, demonstrate that, for the lowest ALMR, the breakup length becomes very long and the liquid jet velocity can become higher than the air flow velocity, which reduces fast as the air jet diffuses. Thus, the transfer of energy is from the liquid to the air stream, and, as a consequence, $U_{detaching}$ can be lower than the liquid nozzle velocity U_L leading to low negative value of SKEI, as observed in Fig.13 for lowest value of ALMR. However, for these conditions, the transfer of energy from the liquid to the air remains small, as expected.

Another important observation of Fig. 13 is that SKEI remains nearly insensitive to the liquid jets impingement angle, as seen for angles 90 and 120°. This finding supports the conclusion from Fig. 12(b), namely that the spatially-averaged droplet size of the sprays did not change

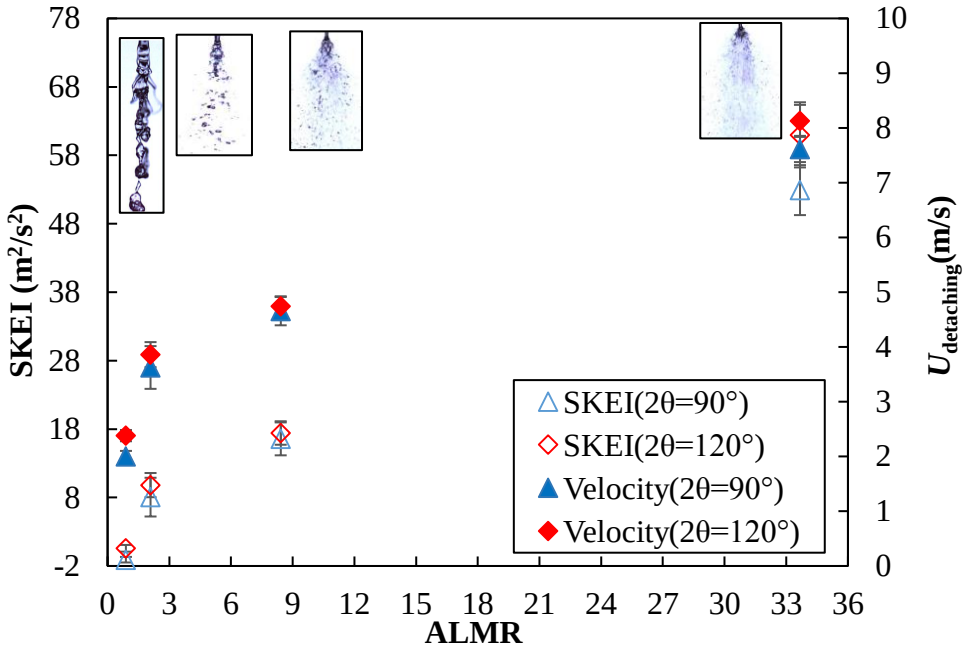


Fig.13. Specific kinetic energy increase (SKEI) before the liquid jets breakup of Eq. (9) and velocity of the liquid at the point where the liquid jet becomes discontinuous $U_{detaching}$ as a function of air-to-liquid momentum ratio ALMR for liquid jets impingement angle 2θ of 90° and 120°.

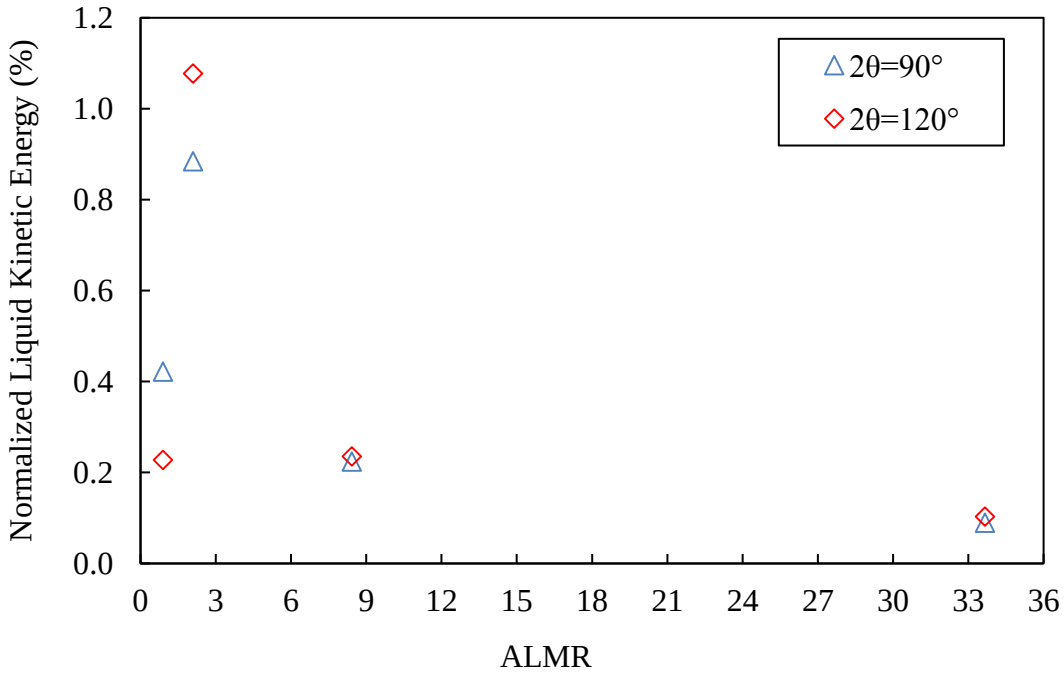


Fig.14. Liquid kinetic energy increase before the breakup location normalized by the air jet kinetic energy, defined in Eq. (10), as a function of air-to-liquid momentum ratio ALMR for liquid jets impingement angle 2θ of 90° and 120°. Note that the mass flowrate of the liquid is the sum of the flowrates supplied to the two liquid jets.

with the increase of the liquid jets impingement angle. Therefore, the breakup process of the liquid and the energy exchange between the air and liquid streams before the breakup of the liquid jets determines the atomization quality and the atomization efficiency.

Since the air kinetic energy contributes to the atomization process, we would like to quantify the amount of energy that has been transferred from the air to the liquid streams *before breakup*. As a consequence, the normalized liquid kinetic energy increase is calculated as shown in Eq. (10):

$$\frac{\dot{m}_L(U^2_{\text{det}aching} - U^2_L)}{\dot{m}_G U^2_G} \times 100\% \qquad (10)$$

which provides a percentage fraction of the air kinetic energy that has been transferred to the liquid *before breakup*. Figure 14 shows that the transferred energy to the liquid from the air stream increased for low ALMR values to a maximum of around 1.1% for ALMR = 3 and, for ALMR>3, the value was reduced to around 0.2% for ALMR = 9 and reduced further slowly to around 0.1% for the maximum ALMR value of 34. These results demonstrate that there is a small fraction of energy transferred from the air to the liquid *before primary breakup* for low ALMR values and, beyond ALMR = 3, the relative transfer becomes very small. These small energy transfers of Fig. 14 justify the behavior of the atomization quality of Fig. 12(c), which changes only by small amount for low values ALMR. The exchange of the kinetic energy between the air and liquid streams depends on the surface of the liquid interface *before breakup*, which is limited. For large values of ALMR, the energy transfer becomes very small because the breakup length becomes short and there is less surface area of liquid interface to transfer energy from the air to the liquid. Therefore, the kinetic energy of the air cannot be used to atomize the liquid and the atomization efficiency is reduced. However, the absolute values of the kinetic energy transfer remain nearly constant for ALMR>3, as shown in Fig. 13, which is enough to deliver the observed atomization quality. This suggests that most of the transferred energy from the air to the liquid *before breakup* is used to increase the surface area of the liquid and generate the initial ligaments at the breakup region, which does not change with the jet impingement angle. Then, some of the kinetic energy of the air is used to accelerate the droplets and for the secondary breakup of the ligaments that were formed during the primary breakup. This leads us to consider the behavior of the atomization efficiency further.

The atomization efficiency, by considering the definitions of Lefebvre (1992) and Pizziol et al. (2018) of Eq. (1) and (2) respectively, is now evaluated. As explained earlier, C* of Eq. (1) represents the fraction of the kinetic energy of the air stream being used for atomization. The present results allow the quantification of C^* for round jets, while considering the spatially-averaged SMD of the sprays for the first time to yield more accurate prediction.

Figure 15 displays the constant C^* using the present set of experimental results, which, for the first time, provide the spatially-averaged SMD in the sprays and ensure that the contribution of all droplets is considered. Two data sets are seen in the figure, which consider the cases of one or two liquid jets interacting with the single air jet and the results are plotted as a function of the Air-to Liquid mass ratio (ALR), calculated on the basis of one and two liquid jets. ALR varies between 0.0032 and 0.0055 for one jet and 0.0058 and 0.105 for two jets. The value of C*=0.007 (or 0.7%), identified by Lefebvre (1992) for the case of a plane liquid sheet, fits within the observed range of values of Fig. 15. The results demonstrate that the atomization efficiency, the portion of the air energy used for atomization, is indeed small, in agreement with the observations made above on energy exchange between the two streams of Fig. 14.

Following Knoll and Sojka (1992) by assuming that C* behavior is dictated by air velocity, ALR and liquid viscosity and using the same arguments put forward by these authors on the functional variations of C* with these variables which are still valid, we also propose a correlation for C* in Equ. (11):

$$C^* = \frac{0.9}{U_G^{1.42\pm0.2} ALR^{0.82\pm0.4} \mu_L^{0.3}} \tag{11}$$

This correlation, which remains valid for the conditions of these experiments, is also presented on Fig. 15 and the agreement is excellent.

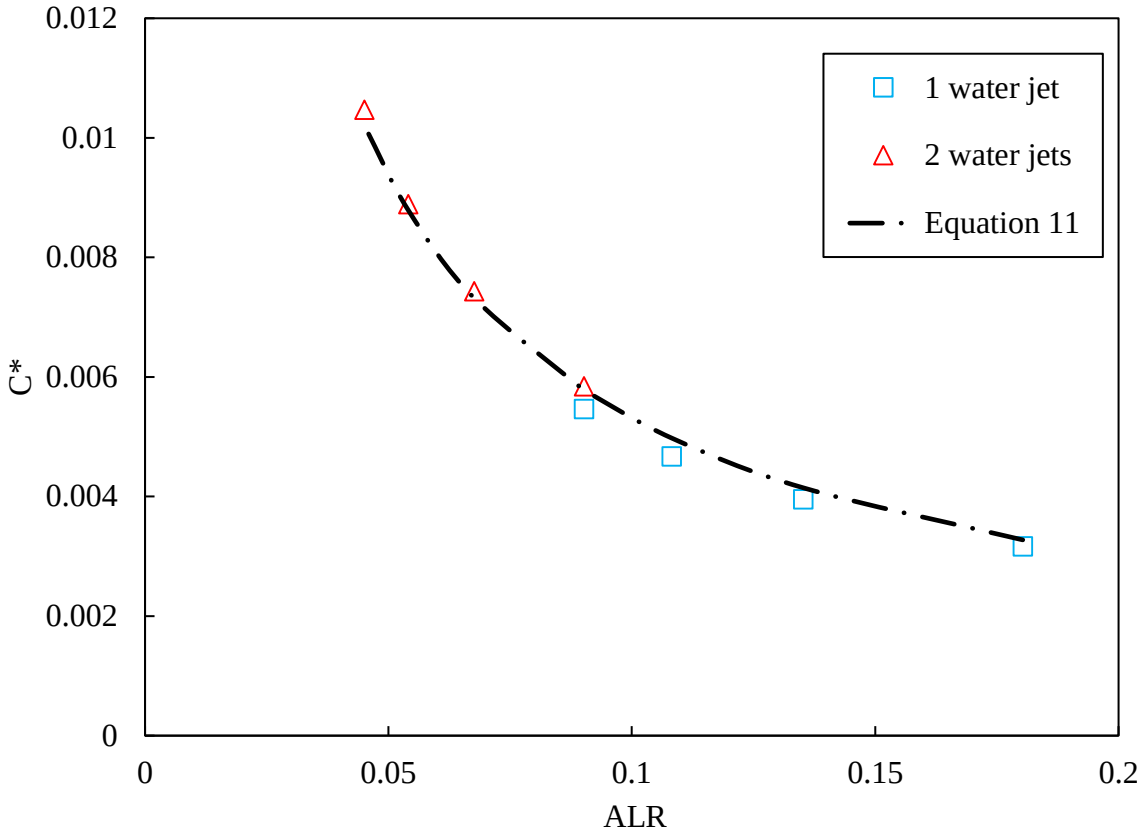


Fig.15. The atomization efficiency, represented by constant C^* of Eq. (1) according to Lefebvre (1992), as a function of ALR for the impinging jet atomizer with impingement angle 2θ = 90°, based on interaction between one liquid or two liquid jets with the single air jet.

Using the spatially-averaged SMD of this work and the local centerline SMD, reported by Xia et al. (2017), Figure 16 presents the atomization efficiency against ALR, according to Eq. (2) based on Pizziol et al. (2018) and includes their results as well. There is overall good agreement between the findings of Pizziol et al. (2018) and the current research, given the changes in the atomizer geometry and the fact that Pizziol et al. (2018) used jet fuel A-1 instead of water of the current study. However, the atomization efficiency is quite high when considering the measured energy exchange between the two streams of Fig. 14 and this is discussed further below. A further observation can be made from Fig. 16 that, although the trends remain the same, the values of the atomization efficiency, based on the spatially averaged SMD, is around 30% lower than those for local centerline SMD for all considered operating conditions.

The results of the current work represent the change of ALR due to the variation of the liquid flowrate, while the air flowrate remains constant for liquid jets impingement angle 2θ =90**°**. First it is important to notice that the results of Pizziol et al. (2018), for jet fuel A-1, indicate

that the efficiency increases for low values of ALR with some scatter and then decreases sharply as ALR increases further. The present results relate to relatively low values of ALR and are thus in agreement with Pizziol et al. (2018), since, in this range of ALR, the efficiency tends to increase rapidly. The atomization efficiency of Pizziol et al. (2018) is of the order of 10% for the current atomizer, while that of Lefebvre (1992) is around 0.7%. The former value is significantly larger than the measured kinetic energy transfer from the air to the liquid, which has a maximum of around 1.1% of the kinetic energy of the air, as shown in Fig. 14. This may be due to the additional energy transfer from the air to the liquid during secondary breakup of the ligaments to form the final droplet sizes in the spray. In addition, it is important to mention that the atomization regime taking place is termed the " fiber regime" in Lasheras and Hopfinger (2000) and is documented in detail in Xia et al. (2017), while the majority, if not all, of the results of Pizziol work for the twin-jet air-assisted geometry take place under a regime dominated by aerodynamic forces where breakup mode is of shear type, which is similar to the present one and it thus suggest that atomization regime discrepancies are not significant to explain the difference in atomization efficiencies between Lefebvre (1992) and Pizziol et al. (2018). However, additional considerations of the assumptions used by Pizziol et al. (2018) and Lefebvre (1992) in the derivation of their expressions are required.

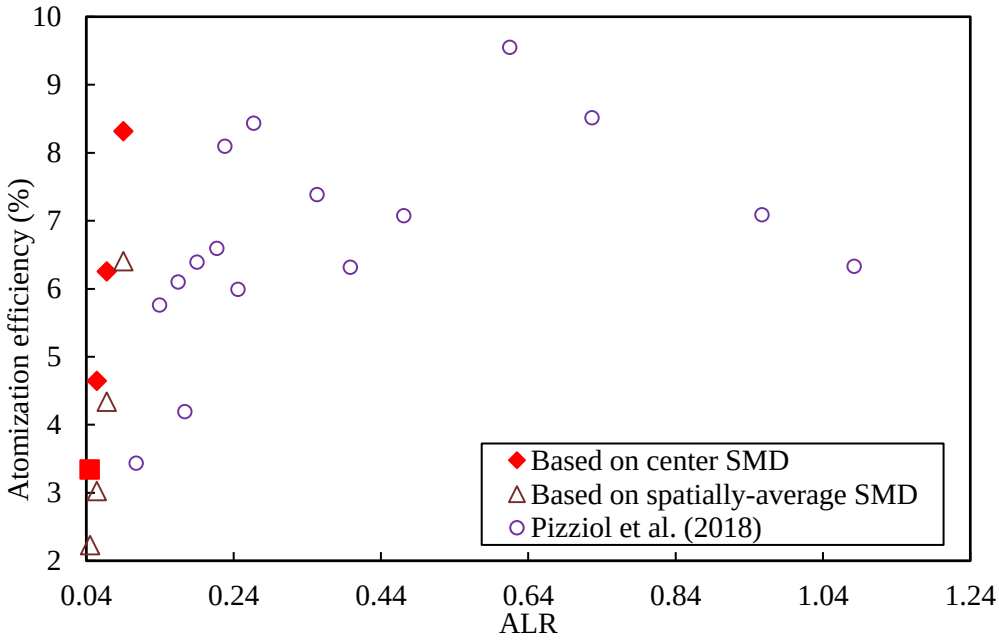


Fig.16. Atomization efficiency, according to Eq. (2) - based on Pizziol et al. (2018), as a function of air to liquid mass flowrate ALR.

The source of differences and deficiencies in both expressions are difficult to identify. Nonetheless, the current research demonstrated the importance of the energy transfer between the air and liquid upstream of the breakup location, which has the ability to explain the observed behavior of the atomization quality and atomization efficiency of atomizers. Fluid computations of atomization using advanced methods may be able to shed more light on the physics of energy transfer between the air and liquid streams to establish an accurate expression of the atomization efficiency.

4. Conclusions

The atomization characteristics at the near nozzle region and the downstream spray characteristics of an atomizer with twin impinging water jets and an air jet were investigated using high-speed photography and PDPA respectively. The following conclusions are extracted:

At the near nozzle region, the normalized breakup length and separation distance of the two liquid jets close to the geometrical 'impingement' region vary rapidly with increasing ALMR and become constant for ALMR > 9. Breakup length normalized by the water jet diameter agrees with existing correlations for co-axial airblast atomizers, and suggests that ALMFR $\approx$ 2 is a threshold above which the air jet penetration through the liquid columns ceases to have an effect on interface topology change. The spray angle in the near nozzle region on the X-Z plane scales with ALMR for different air mass flowrates and is not sensitive to the liquid jets impingement angle.

The droplet SMD, axial velocity and normalized liquid volume flux of the downstream sprays indicated that the spray spreads over a wider region with increasing water flowrates with the minimum and maximum values of the SMD remaining almost the same at 60μm and 120 μm respectively. The measured value of SMD in the central part of the spray agrees with the estimate provided by the correlation of Sallam et al. (2004).

A spatially-averaged SMD was used to quantify the atomization quality for the first time and found to be independent of the liquid jets impingement angle, which demonstrated that local SMD profiles, although necessary, are not sufficient to draw conclusions on the atomization quality. In addition, the atomization quality was found to change by only 5.6% for a change of the ALMR by a factor of nearly 4. The small change of the atomization quality is a surprising finding that could only be obtained from the measured spatially-averaged droplet diameter of the current work.

The measured relative value of the energy transfer from the air to the liquid streams before the breakup location increased to around 1.1 % of the supplied air flow kinetic energy for ALMR=3, reduced to around 0.2% for ALMR=9 and slowly reduced to 0.1% for ALMR=34 and was independent of the liquid jets impingement angle. This was in agreement with the measured small changes of the atomization quality and remained also independent of the impingement angle.

A correlation was proposed for the atomization efficiency similar to the one proposed by Knoll and Sojka (1992) providing excellent agreement with measured data. The atomization efficiency was quantified from the measured spatially-averaged SMD, for the first time and according to formalisms of Lefebvre (1992) and Pizziol et al. (2018). Based on the latter, the atomization efficiency increased with the reduction of the liquid flowrate and increase of air flowrate up to Air-to-Liquid mass flowrate Ratio (ALR) of 0.2 beyond which further increase leads to reduction of efficiency. This trend did not agree with Lefebvre, but the values of the atomization efficiency of Lefebvre's formalism were around 0.7% of the supplied air kinetic energy, in agreement with the measured energy exchange between the air and liquid streams *up to the primary breakup* of the current work, in contrast to the larger values of Pizziol et al. which may be justified by the additional transfer of energy during the secondary breakup of ligaments. In the light of this work, which demonstrated that the energy transfer between the air and liquid streams in the near nozzle region affects the behavior of the atomization quality and efficiency of the atomizer, the assumptions of the formalisms of Lefebvre (1992) and Pizziol et al. (2018) must be reconsidered.

Acknowledgements

The authors gratefully acknowledge the support from Khalifa University of Science and Technology, Abu Dhabi, UAE in the form of a visiting graduate research assistant grant to Y. Xia. They are also thankful to the suggestions made by the reviewers in improving the manuscript.

References

Ashgriz, N., Impinging jet atomization, Handbook of Atomization and Sprays, Springer, pp. 685-707, 2011.

Avulapati, M.M. and Ravikrishna, R.V., Experimental studies on air-assisted impinging jet atomization, Int. J. Multiphase Flow. 57, pp. 88-101, 2013.

Avulapati, M.M. and Ravikrishna, R.V., Experimental studies on air-assisted atomization of Jatropha pure plant oil, Atomization Sprays. 25(7), pp. 553-569, 2015.

Beck, J.E., Lefebvre, A.H. and Koblish, T.R., Liquid sheet disintegration by impinging ait streams, Atomization and Sprays. 1(2), pp. 155-170, 1991.

Boden, J.C., Hardalupas, Y., Krenteras, P., Taylor, A.M.K.P., Spray characteristics from free impinging air and liquid jets. Proc. 15th ILASS-Europe, Toulouse, 1999.

Collins, T.J., ImageJ for microscopy, Biotechniques, 43(1 Suppl), pp. 25-30, 2007.

Cossali, E. and Hardalupas, Y., Comparison between laser diffraction and phase Doppler velocimeter techniques in high turbidity, small diameter sprays, Expts in Fluids 13, pp. 414 – 422, 1992.

Dombrowski, N. and Hooper, P., A study of the sprays formed by impinging jets in laminar and turbulent flow, J. Fluid Mech., 18, pp. 392-400, 1964.

Engelbert, C., Hardalupas, Y., Whitelaw, J.H., Breakup phenomena in coaxial airblast atomizers, Proc. R. Soc. Lond. A451, pp. 189-229, 1995.

Eroglu, H., Chigier, N., Farago, Z., Coaxial atomizer liquid intact lengths, Phys. Fluids A-Fluid. 3(2), pp. 303-308, 1991.

Hardalupas, Y., Taylor, A.M.K.P., Whitelaw, J.H., Velocity and particle-flux characteristics of turbulent, particle-laden jets, Proc. R. Soc. Lond. A426, pp.31 -78, 1989.

Hardalupas, Y., Taylor, A.M.K.P. Whitelaw, J.H., Mass flux, mass fraction and concentration of liquid fuel in a swirl-stabilized flame, Int. J. Multiphase Flow. 20, pp. 233-259, 1994.

Inoue, C., Watanabe, T. Himeno, T., Uzawa, S., Impinging Atomization Enhanced by Microjet Injection-effect, mechanism and optimization, 49th AIAA/ASME/SAE/ASEE Joint Propulsion Conference 3705, 2013.

Knoll, K.E. and Sojka, P.E., Flat-sheet twin-fluid atomization of high viscosity fluids. Part I: Newtonian liquids. Atomization and Sprays, 2, pp.17-36, 1992.

Lai, W., Shakal, J., Troolin, D., Accuracy, resolution and repeatability of powersight PDPA and LDV systems, TSI Technical Note P. (5001520) A4, 2013.

Lasheras, J.C., and Hopfinger, E., Liquid jet instability and atomization in a coaxial gas stream, Annu. Rev. Fluid Mech. 32(1), pp. 275-308, 2000.

Lefebvre, A.H., Energy considerations in twin-fluid atomization, J. Eng. Gas Turb. Power, 114, pp. 89-96, 1992.

Leroux, B., Delabroy, O., Lacas, F., Experimental study of coaxial atomizers scaling, Part I: dense core zone. Atomization Sprays. 17(5), pp. 381-407, 2007.

Panao, M.R.O. and Delgado, J.M.D., Towards the design of low flow-rate multijet impingement spray atomizers, Exp. Therm. Fluid Sci. 58, pp. 170-179, 2014.

Pizziol, B., Costa, M., Panao, M.O., Silva, A., Multiple impinging jet air-assisted atomization, Exp. Therm. Fluid Sci. 96, pp. 303-310, 2018.

Prabhakaran, P. and Basavanahalli, R., Gas-on-Liquid Impinging Injectors: Some New Results, 49th AIAA/ASME/SAE/ASEE Joint Propulsion Conference 3706, 2013.

Ramasubramanian, C., Notaro, V. Lee, J.G., Characterization of Near-Field Spray of Nongelled-and Gelled-Impinging Doublets at High Pressure, J. Propul. Power., 31(6), pp. 1642-1652, 2015.

Sallam, K.A, Aalburg, C., Faeth, G.M., Breakup of round non turbulent liquid jets in gaseous crossflow, AIAA J. 42, pp. 2529–2540, 2004.

Schneider, C.A., Rasband, W.S., Eliceiri, K.W., NIH Image to ImageJ: 25 years of image analysis, Nature methods. 9(7), pp. 671, 2012.

Sommerfeld, M. and Qiu, H.H. Particle concentration measurements by phase-Doppler anemometry in complex dispersed two-phase flows, Exp. Fluids. 18 (3), pp. 187-198, 1995.

Spalding, D.B., Combustion and mass transfer (1st Ed.), Pergamon Press, Oxford, 1979.

Xia, Y., Khezzar, L., Alshehhi, M., Hardalupas, Y., Droplet size and velocity characteristics of water-air impinging jet atomizer, Int. J. Multiphase Flow. 94, pp. 31-43, 2017.

Xia, Y., Alshehhi, M., Hardalupas, Y., Khezzar, L., Spray characteristics of free air-on-water impinging jets, Int. J. Multiphase Flow. 100, 86-103, 2018a.

Xia, Y., Khezzar, L., Alshehhi, M., Hardalupas, Y., Atomization of impinging opposed water jets interacting with air jet, Exp. Therm. Fluid Sci. 93, pp. 11-22, 2018b.